

Air Force Institute of Technology

AFIT Scholar

Theses and Dissertations

Student Graduate Works

3-15-2006

Optical Characterization of Thick Growth Orientation-Patterned Gallium Arsenide

Joshua W. Meyer

Follow this and additional works at: <https://scholar.afit.edu/etd>



Part of the [Semiconductor and Optical Materials Commons](#)

Recommended Citation

Meyer, Joshua W., "Optical Characterization of Thick Growth Orientation-Patterned Gallium Arsenide" (2006). *Theses and Dissertations*. 3356.
<https://scholar.afit.edu/etd/3356>

This Thesis is brought to you for free and open access by the Student Graduate Works at AFIT Scholar. It has been accepted for inclusion in Theses and Dissertations by an authorized administrator of AFIT Scholar. For more information, please contact AFIT.ENWL.Repository@us.af.mil.



**OPTICAL CHARACTERIZATION OF THICK GROWTH
ORIENTATION-PATTERNED GALLIUM ARSENIDE**

THESIS

Joshua W. Meyer, Captain, USAF

AFIT/GAP/ENP/06-10

DEPARTMENT OF THE AIR FORCE
AIR UNIVERSITY

AIR FORCE INSTITUTE OF TECHNOLOGY

Wright-Patterson Air Force Base, Ohio

APPROVED FOR PUBLIC RELEASE; DISTRIBUTION UNLIMITED

The views expressed in this thesis are those of the author and do not reflect the official policy or position of the United States Air Force, Department of Defense, or the United States Government.

AFIT/GAP/ENP/06-10

OPTICAL CHARACTERIZATION OF THICK GROWTH
ORIENTATION-PATTERNED GALLIUM ARSENIDE

THESIS

Presented to the Faculty
Department of Engineering Physics
Air Force Institute of Technology
Air University
Air Education and Training Command
In Partial Fulfillment of the Requirements for the
Degree of Master of Science (Applied Physics)

Joshua W. Meyer, B.A.

Captain, USAF


March 2006

APPROVED FOR PUBLIC RELEASE; DISTRIBUTION UNLIMITED

OPTICAL CHARACTERIZATION OF THICK GROWTH
ORIENTATION-PATTERNED GALLIUM ARSENIDE

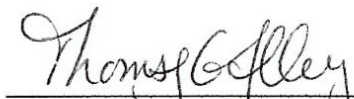
Joshua W. Meyer, B.A.
Captain, USAF

Approved:




Matthew J. Bohn (Chairman)

14 Mar 06
date



Thomas G. Alley (Member)

14 Mar '06
date



Rita D. Peterson (Member)

15 Mar 06
date

Abstract

Tunable laser sources in the mid-infrared (MIR) spectral range are required for several Air Force applications. Existing lasers with output in the near-infrared can be converted to more desirable MIR by using nonlinear effects. Orientation patterned gallium arsenide (OPGaAs) is a promising nonlinear conversion material because it has broad transparency and can be engineered for specific pump laser and output wavelengths using quasi-phase matching techniques. This research examines the optical quality of seven OPGaAs crystal samples and explores the design of an optical parametric oscillator (OPO) device. The Air Force Research Laboratory Electro-Optical Countermeasures Technology Branch obtained the samples from two independent, industrial suppliers. Direct transmission and scattering measurements at 2.05- μm were taken as a function of position across the incident face of each sample. Scattering, absorption, and reflection coefficients for each sample were quantified. The sample with the most favorable coefficients was selected for use in an OPO. Nonlinear output from the OPO was not achieved before the optical coating failed. A direct comparison of OPGaAs crystal performance based on source of manufacturing is reported. Results are discussed to aid in improvements to OPGaAs fabrication techniques. Optical quality data are graphically presented to illustrate total performance resulting from crystal design features. OPO design parameters are summarized with recommendations for future efforts.

Acknowledgements

This project and the AFIT curriculum have been the most difficult challenges I've encountered during my nearly 10 years of military service. Many thanks are in order to those people who assisted in this endeavor. First and foremost I want to sincerely thank my research sponsor, Dr. Rita Peterson, whose guidance, encouragement, and expertise allowed me to successfully complete this program.

Additionally, I wish to express my appreciation to my faculty advisor, Lt Col Matthew Bohn, for his keen insight, focus on the big picture of which I needed occasional reminding, and for his professional career advice.

I also gratefully acknowledge the support of Northrop-Grumman Corp. and BAE Systems Inc. through the CARMA effort (F33615-02-2-1111 and F336715-02-2-1110), for providing the samples used in my research.

Finally, all my love goes to my admirable wife and two wonderful daughters for their patience and support during this 18-month journey.

Joshua W. Meyer

Table of Contents

	Page
Abstract	iv
Acknowledgements	v
List of Figures	vii
List of Tables	ix
I. Introduction.....	1
1. Motivation	1
2. Overview	4
II. Background.....	5
1. Advantages of OPGaAs.....	5
2. Nonlinear Optical Theory.....	6
3. Quasi-Phase Matching.....	10
4. Previous Work.....	11
5. Fabricating OPGaAs.....	13
III. Experiments.....	16
1. OPGaAs Samples	16
2. Pump Laser.....	21
3. Power Transmission Experiment.....	24
4. Scattering Experiment	26
5. Reflection Experiment.....	30
6. OPO Experiment	31
IV. Data and Analysis.....	34
1. Reflection Losses	34
2. Scattering and Absorption Losses	34
3. OPGaAs OPO.....	48
V. Conclusions and Recommendations	50
1. Conclusions	50
2. Recommendations	50
Appendix	53
Bibliography	55
Vita	58

List of Figures

Figure	Page
1: Optical parametric processes.	7
2: Comparison of phasematching techniques.	11
3: OPGaAs growth process	14
4: Magnified image of sample 6.	18
5: View of upper surfaces of samples.	19
6: Sample 2 close up picture	20
7: Sample 6 close up picture	20
8: Sample coating performance plot.	21
9: Tm,Ho:YLF pump laser	22
10: Pump laser beam waist profile	23
11: Pump beam intensity profile.	24
12: Depiction of pump beam probe pattern along face of OPGaAs samples.	26
13: Scattering measurement setup.	27
14: Photograph of integrating sphere assembly.	28
15: Integrating sphere interior detail.	29
16: Tm,Ho:YLF pumped OPO cavity	32
17: InGaAs detector response.	35
18: Sample 1 losses.	39
19: Sample 2 losses.	40
20: Sample 3 losses.	41
21: Sample 4 losses.	42

Figure	Page
22: Sample 5 losses.....	43
23: Sample 6 losses.....	44
24: Sample 7 losses.....	45
25: Beam propagation through sample 2.	53
26: Beam propagation through sample 5.	54

List of Tables

Table	Page
1: Material comparisons.....	6
2: Description of OPGaAs samples.	17
3: Measured reflection coefficients of all samples.	34
4: Indirect absorption per sample.....	36
5: Loss coefficients summary	46

OPTICAL CHARACTERIZATION OF THICK GROWTH ORIENTATION-PATTERNED GALLIUM ARSENIDE

I. Introduction

There is a growing interest by government officials in mid-infrared laser applications such as countermeasures against man portable air defense systems and remote environmental sensing to include detection and identification of chemicals. Additional defense specific applications using laser output in the 2- μm to 5- μm wavelength region include target acquisition, recognition, and designation. These applications require tunable, efficient, and reliable laser sources. To date, the shortage of acceptable laser sources for these applications continues to press for better solutions. In order to achieve the desired wavelengths, nonlinear optical devices are used to alter the wavelength of an existing laser in order to produce energy at an advantageous wavelength. One such nonlinear device is called an optical parametric oscillator (OPO). An OPO, while still limited by available materials, allows for tuning of the projected beam across a much greater spectral range than typical solid state lasers.

1. Motivation

An undesirable wavelength and insufficient tunability are primary reasons non-linear optical materials and techniques like OPO and orientation patterned gallium arsenide (OPGaAs) are in demand. Current materials used in or considered for military defense applications, like periodically-poled lithium niobate (PPLN), silver gallium selenide

(AgGaSe₂), and zinc germanium phosphide (ZGP) all have desirable features, yet each has limiting factors.

Lithium niobate has been used in the design of OPOs since the early 1960's (Giordmaine and Miller, 1965:973-975). It is a ferroelectric material allowing the polarity of the crystal to be easily and permanently reversed in a periodic manner by applying a large voltage across the LiNbO₃ crystal (Myers and others, 1995:2102-2116). Periodically-poled LiNbO₃ and other ferroelectric materials are a good choice for current infrared countermeasure (IRCM) devices due to years of testing, ease of manufacturing, and tunability across a wide spectral range. However, they all have a significant drawback of performance degradation when operated at wavelengths longer than 4- μ m due to absorption.

Silver gallium selenide has two optimal characteristics for a nonlinear device. It has a broad transparency region extending to 11- μ m allowing for a wide range of OPO output frequencies. Also, AgGaSe₂ has a high d_{eff} value which positively impacts the overall gain efficiency of the OPO. However, an OPO based on AgGaSe₂ does not reach optimal output power levels due to an inability to dissipate damaging waste heat. This waste heat results in thermal lensing causing limitations to the output power level (Zeigler and Schepler, 1991:5077; Budni and others, 2000:723-728).

Zinc germanium phosphide (ZGP), like AgGaSe₂, has a large d_{eff} , (Vodopyanov and others, 2000:842), but is not as transmissive as OPGaAs with a transmission range from 2- μ m to 8- μ m (Peterson and others, 1995:2142). ZGP and AgGaSe₂ are both birefringent materials while GaAs is not. Birefringent materials have a refractive index that depends on the polarization and direction of the light that passing through them. Natural

birefringent materials introduce a complexity into nonlinear device design since the propagating pump beam must maintain an exacting polarization angle relative to the crystal axis in order to achieve desired output characteristics. Tuning of the output occurs when the relative angles are altered, a technique called angle tuning. Angle tuning has a limitation since the beams propagate at slightly different angles causing the extraordinary wave to experience Poynting vector walk-off. If the beam size of the input laser is small, as is the case in these experiments, the generated beam and input beam will be separated at a walk-off angle in a birefringent crystal reducing conversion efficiency and output power while increasing the M^2 value of the laser. For nonlinear cavities using a focused beam, Poynting vector walk-off is a limiting factor to high efficiency (Principles, 2005). Some compensation for pointing vector walk-off can be achieved by use of a second birefringent material placed so the crystal orientation is reversed compared to the first crystal (Setzler and others, 2002:85).

Orientation patterned gallium arsenide is an important area of research in IRCM and remote sensing applications. Its transparency range is broader than most materials and OPO performance promises output power levels desirable for military applications. Using the nonlinear optical qualities of OPGaAs promises an increase to sensor and IRCM capabilities on the battlefield. It may give battlefield commanders greater operational flexibility and free up personnel and assets for other priority missions.

The Air Force Research Laboratory Electro-Optics Branch obtained several OPGaAs crystal samples through ongoing contractual efforts for demonstrating a 2.05- μm pumped nonlinear laser device. The objective of this work was to report comparisons of OPGaAs samples with thicknesses sufficient for OPO device demonstration originating from

different suppliers. A secondary objective was to design and test an OPO using one or more of the OPGaAs samples.

2. *Overview*

The objective of this research effort was to measure and describe the optical quality of multiple OPGaAs samples in order to provide feedback to manufacturing engineers with the goal of improving future crystal growth. OPGaAs engineering techniques have improved in recent years leading to fabrication of thicker samples with higher optical quality. The effort of this research concentrated on detailed optical loss analysis for each of the seven samples at $2.05\mu\text{m}$ wavelength. Results of the measurements led to the design and testing of an OPO.

Chapter II of this thesis discusses relevant theory of physical processes occurring in nonlinear optical devices. A section is included outlining methods used in the fabrication of OPGaAs. In addition, a chronological account of previous work of others in this area is given. Chapter III details the seven OPGaAs samples used in the experiments and the $2.05\text{-}\mu\text{m}$ Tm,Ho:YLF laser used for pumping them. Additionally, experimental designs for measuring power transmission, absorption, and reflection are described. Finally, the design and operation of the OPO is covered. Chapter IV presents the results of the all experiments. Although the OPO demonstration was unsuccessful, recommendations from the experiment should add to the body of knowledge concerning OPGaAs OPO design. Chapter V offers final conclusions and recommendations for future work with these and similar OPGaAs samples.

II. Background

1. Advantages of OPGaAs

Since the 1960's researchers have continued to identify and design materials for nonlinear optical frequency conversion although many do not possess the most desirable characteristics for an OPO. The characteristics include the ability to phase-match, an extended transparency range, a large nonlinear susceptibility and high damage thresholds (Harris, 1969:2097). Gallium arsenide (GaAs) possesses many of these desirable characteristics. Its transparency window is from 1- μm to 16- μm , the damage threshold is relatively high (Wolfe, 1993:22). It has a relatively high second order nonlinear coefficient, d_{eff} , compared to other materials used for similar applications. A comparison of d_{eff} values and transparency windows for several materials is shown in Table 1. The properties of GaAs are well understood and supply sources are plentiful since it is a commonly used material in the semiconductor and communications industries. A well known and obtainable material is often preferable to a rare, untested material when considering applications in military systems due to lower associated risk.

Despite a list of advantageous characteristics, GaAs is a crystal with cubic symmetry, it is an isotropic material with respect to its index of refraction, and it is not ferroelectric. Isotropic materials, lacking birefringence, must find methods other than angle-tuning to achieve phase matching for efficient parametric output. One method is to engineer a pattern into the isotropic material. A proven method of producing patterns in materials using intense static electric fields, i.e. poling, only works on ferroelectric crystals. These issues are discussed in greater detail in subsequent sections.

Table 1: Material comparisons.

(Fejer, 2004:n. pag.)

	GaAs	GaP	ZnSe	InAs	InP	ZGP	PPLN
d_{eff} (pm/V)	110	37	50	300	140	70	28
Transparency (μm)	1-16	0.6-11	0.5-22	3.8-7	1-14	0.7-11	.35-4.5

2. *Nonlinear Optical Theory*

Nonlinear Parametric Process: Several texts are excellent resources on theories of quasi-phase matching and OPO design. Following the development shown in Yariv and Yeh ; an overview of nonlinear theory follows while an extension to it can be found in other writings (Yariv and Yeh, 1984; McMullen, 1975:3076-3081).

Second order, χ^2 , nonlinear parametric processes occur when three photons interact. Boyd describes nonlinear effects as occurring when “the response of a material system to an applied optical field depends in a nonlinear manner” upon the input electromagnetic wave (Boyd, 1992:6). With respect to OPO processes, the photon with the highest energy is designated as the pump photon. The signal and idler photons refer to the two remaining photons. In an OPO, the pump photons are converted into signal and idler photons. This nonlinear process is realized when two fundamental laws are met: conservation of energy and conservation of momentum. Mathematically, conservation of energy of the pump, signal, and idler photons is described by

$$\frac{h}{2\pi} \omega_{\text{pump}} = \frac{h}{2\pi} \omega_{\text{signal}} + \frac{h}{2\pi} \omega_{\text{idler}} \quad (1)$$

where h is Planck's constant, and ω is the angular frequency.

When a pump photon with an intense electric field and frequency, ω_{pump} , enters a nonlinear crystal, the polarization, or dipole moment per unit volume, of the crystal is altered. The material's nonlinear polarization can produce electromagnetic radiation at additional frequencies (ω_{idler} and ω_{signal}) provided energy and momentum are conserved. A representative nonlinear parametric process is depicted in Figure 1.

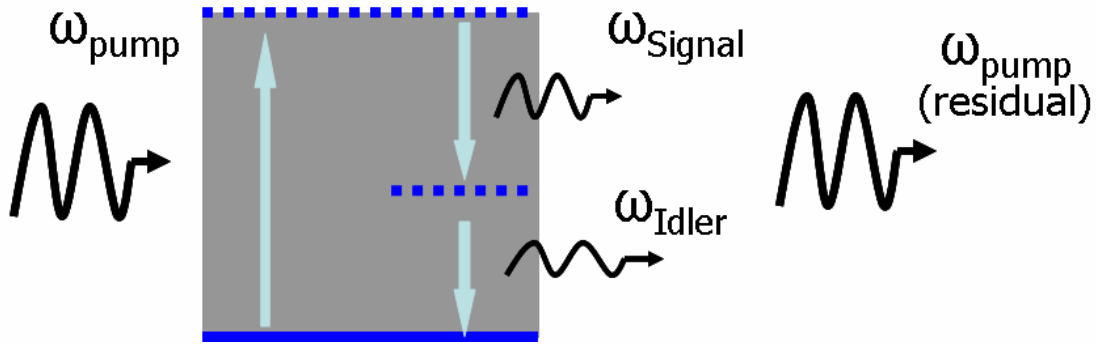


Figure 1: Optical parametric processes.

The idler and signal frequencies gain energy from the pump frequency. All three frequencies propagate out of the system. In a singly resonant oscillator, the idler does not resonate and propagates without reflection, whereas a doubly resonant oscillator defines a cavity in which both idler and signal frequencies are resonant or the pump and signal frequencies are resonant.

In addition to conservation of energy, momentum must also be conserved. The wavevector, \vec{k} , of each wave is used to balance the momentum relationship and form a conditional requirement known as phase matching expressed as

$$\frac{h}{2\pi} \vec{k}_{pump} = \frac{h}{2\pi} \vec{k}_{signal} + \frac{h}{2\pi} \vec{k}_{idler} \quad (2)$$

The origin of this requirement can be seen in the following derivation. Beginning with Maxwell's Equations (in MKS units) the nonlinear wave equation is:

$$\nabla^2 \bar{E} \cong \mu_0 \sigma \frac{\partial \bar{E}}{\partial t} + \mu_0 (\varepsilon_0 + \varepsilon_0 \chi_L) \frac{\partial^2 \bar{E}}{\partial t^2} + \mu_0 \frac{\partial^2 \bar{P}_{NL}}{\partial t^2} \quad (3)$$

where μ_0 is the permeability of free space, ε_0 is the permittivity of free space, $\nabla^2 \bar{E}$ is the Laplacian of the electric field, χ_L is the scalar susceptibility, and σ represents losses. The polarization vector has a linear and nonlinear component such

that $\bar{P} = \bar{P}_L + \bar{P}_{NL}$. It is important to note the term $\mu_0 \frac{\partial^2 \bar{P}_{NL}}{\partial t^2}$ in Equation 3 is the driving term.

Assuming plane wave propagation along the z-axis, the pump, signal, and idler beams with frequencies ω_1 , ω_2 , and ω_3 respectively, can be represented as

$$\begin{aligned} E_{pump-x,y}(\omega_1) &= \frac{1}{2} \left[E_{pump-x,y}(z) e^{i(k_1 z - \omega_1 t)} + E_{pump-x,y}(z) e^{-i(k_1 z - \omega_1 t)} \right] \\ E_{signal-x,y}(\omega_2) &= \frac{1}{2} \left[E_{signal-x,y}(z) e^{i(k_2 z - \omega_2 t)} + E_{signal-x,y}(z) e^{-i(k_2 z - \omega_2 t)} \right] \\ E_{idler-x,y}(\omega_3) &= \frac{1}{2} \left[E_{idler-x,y}(z) e^{i(k_3 z - \omega_3 t)} + E_{idler-x,y}(z) e^{-i(k_3 z - \omega_3 t)} \right] \end{aligned} \quad (4)$$

These expressions for the electric field must satisfy the wave equation, (3) yielding a set of coupled equations for a single pass through a lossy medium:

$$\begin{aligned}
\frac{\partial E_{pump}}{\partial z} &= -\frac{\sigma_{pump}}{2} E_{pump} + i \frac{\omega_{pump} d_{eff}}{n(\lambda_{pump}) c} E_{signal} E_{idler} e^{-i\Delta k_z} \\
\frac{\partial E_{signal}}{\partial z} &= -\frac{\sigma_{signal}}{2} E_{signal} + i \frac{\omega_{signal} d_{eff}}{n(\lambda_{signal}) c} E_{pump} E_{idler}^* e^{-i\Delta k_z} \\
\frac{\partial E_{idler}}{\partial z} &= -\frac{\sigma_{idler}}{2} E_{idler} + i \frac{\omega_{idler} d_{eff}}{n(\lambda_{idler}) c} E_{pump} E_{signal}^* e^{-i\Delta k_z}
\end{aligned} \tag{5}$$

where σ is the electric field loss, d_{eff} is the nonlinear coefficient tensor, and $n(\lambda)$ is the wavelength dependent refractive index. Relationships for threshold intensity and gain are found using an extension to these derivations.

The amount of phase mismatch Δk_z , (the difference of the wave vectors), governs the efficiency of the conversion process. Dropping the subscript z, it is given by

$$\Delta k = k_{pump} - k_{idler} - k_{signal} = \frac{2\pi n_{pump}}{\lambda_{pump}} - \frac{2\pi n_{signal}}{\lambda_{signal}} - \frac{2\pi n_{idler}}{\lambda_{idler}} \tag{6}$$

The above equation is known as the phase matching condition. Equations 1 through 6 describe the second order nonlinear process in most materials. Birefringent phase matching is a technique to obtain phase matching for a nonlinear process by exploiting the birefringence of a nonlinear crystal. Typically, three-wave mixing is done in a birefringent crystalline material where the polarizations of the fields and the orientation of the crystal are chosen such that the phase-matching condition is fulfilled. This phase matching technique permits angle tuning, in which the output wavelengths can be

changed by rotating the crystal relative to the pump propagation direction. One undesirable effect of angle tuning is the extraordinary wave propagating through a birefringent crystal possesses a Poynting vector that is not parallel with the propagation vector which results in the energy deviating, or ‘walk-off’, from the propagation direction and ultimately limits the nonlinear optical conversion efficiency. Walk-off can be avoided if non-critical phase-matching is possible, in which all frequencies propagate at a 90 degree angle with respect to the optical axis of the crystal.

3. *Quasi-Phase Matching*

In QPM, the phase mismatch Δk is not minimized through birefringence, instead the sign of the effective nonlinear coefficient is flipped at a regular interval chosen to equal the phase mismatch that otherwise would be present in the non-patterned crystal. The reversal of the nonlinear coefficient term shifts the polarization response of the crystal back into phase with the pump beam allowing for continued net positive energy flow from the pump into the signal and idler frequencies. The crystal domain period, Λ , also contributes to total momentum of the system. The additional momentum, Λ , can be included in (6):

$$\Delta k = k_{pump} - k_{idler} - k_{signal} - \frac{2\pi}{\Lambda} \quad (7)$$

For first-order quasi-phase matching condition, the domain period is two times the coherence length. The physical distance of each coherence length in a first order QPM is defined by

$$l_{coh} \equiv \frac{\pi}{k_{pump} - k_{signal} - k_{idler}} \quad (8)$$

By reversing d_{eff} every coherence length, the nonlinear interaction continues to grow, albeit not as efficiently as birefringently phase matched materials. Were d_{eff} not reversed, after each l_{coh} energy would flow back into pump leaving no net signal and idler. A lack of phase matching allows energy to flow sinusoidally back and forth between the input and output waves. Figure 2 compares the signal power for these three conditions.

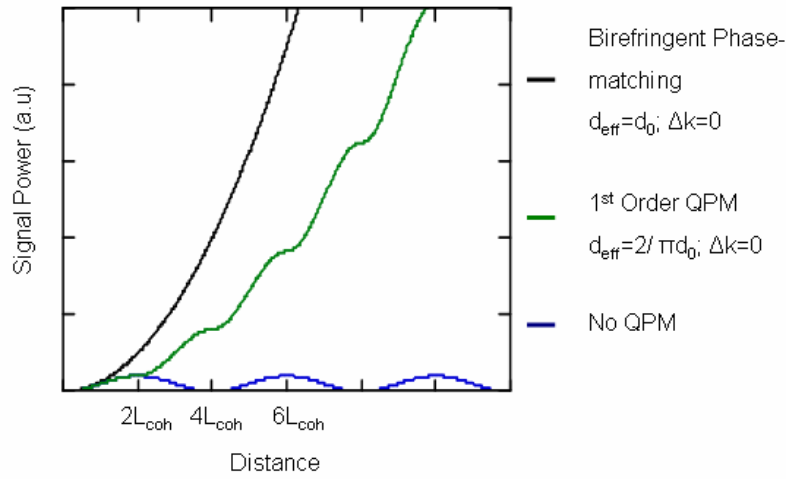


Figure 2: Comparison of phasematching techniques.

4. Previous Work

Since its invention in 1960, the laser has become a valuable device in a variety of applications (Maiman, 1960:493-494). Since the wavelength of the laser is a significant characteristic affecting its utility, it is often desirable to change the output wavelength of the laser to a specific wavelength range. Franken et al. first demonstrated in 1961 the use of nonlinear optical frequency mixing to extend the spectral range of existing lasers when they witnessed the second harmonic generation of a ruby laser (Franken and others, 1961:118). In 1962, the optical parametric oscillator was first proposed (Armstrong and

others, 1960:1918-1939) as a device capable of converting a single frequency laser into a tunable laser source. The first experimental tunable OPO was demonstrated in 1965 (Giordmaine and Miller, 1965:973-976). The first nonlinear optical effect observed in GaAs was second harmonic generation by Thompson and others using a CO₂ laser (Thompson and others, 1976:113).

Recent attempts to achieve nonlinear conversion in OPGaAs have led to an improved understanding of the material. Harm reported that the index of refraction must be accurately known to greater than 0.01% in order to properly design quasi-phasematched GaAs (Harm, 2002:41). Inaccuracies in the index of refraction value resulted in calculating an improper coherence length and fabrication of crystals that wouldn't phasematch. More precise index of refraction values were measured by the Air Force Research Laboratory to further proper QPM design in GaAs.

In 2004, the first OPGaAs OPO was demonstrated (Vodopyanov and others, 2004:1912-1914). A miniature, Q-switched neodymium, yttrium aluminum garnet (Nd:YAG) laser pumped a tunable PPLN OPO. The output from the PPLN OPO passed through a series of filters transmitting 1.8- μm to 2.0- μm wavelengths for use by the OPGaAs sample. The beam, focused to a $1/e^2$ intensity radius of 180- μm passed through an OPGaAs crystal measuring 5mm wide, 11 mm long, and 0.5mm thick. The SRO design reached photon conversion slope efficiency of 54%. SRO threshold was 16- μJ for the 6-ns pump pulses.

Schunemann and others reported the first direct laser-pumped OPGaAs OPO (Schunemann and others: 2005) by successfully demonstrating both a singly-resonant OPO cavity and a doubly-resonant cavity. Their work is closely related to this endeavor

since they used direct-pumping from a 2.05- μm Tm,Ho:YLF source. Using the DRO set up, the highest average power reached was 0.45 watts with a slope efficiency of 20%. Similarly, the SRO design reached a maximum average output power of 0.35 watts with a 20% slope efficiency. Damage occurred to the sample coating at a fluence of 1.35 J/cm².

5. *Fabricating OPGaAs*

Unlike ferroelectric materials, the polarity of semiconductors like GaAs cannot be reversed by simply applying large voltages. Reversing the nonlinear coefficient at regular intervals, i.e. orientation patterning, was first achieved by mechanical means. Slices of gallium arsenide were cleaved from a uniform block. Surfaces were polished; every other slice rotated 180 degrees, and finally reassembled (McMullen, 1975:3076-3080). Assembling patterned GaAs in this manner introduced imperfect interfaces at the plates causing optical losses too high to overcome.

Diffusion bonding, techniques were developed to overcome the high scattering losses (Gordon and others, 1993:1942-1944). The process included heating a stack of GaAs plates under pressure. While the scattering losses were reduced, the technique required the difficult tasks of polishing and manipulation of thin sheets of GaAs.

In 1999, Ebert and others invented a process to fabricate a single crystal containing regions out of phase with each other (Ebert and others, 1999:187-193). They noted that placing a 30 angstrom layer of germanium on top of the initial layer of GaAs, a subsequent layer of GaAs could be added in a reverse orientation (Koh and others, 2001:183-192). The material surface was photolithographically etched through the germanium layer creating a template. Next, molecular beam epitaxy was used to grow the lower layer of GaAs to a thickness of approximately 10- μm .. A device-quality

thickness is reached by using hydride vapor phase epitaxy (HVPE) to continue the periodic structure to a final thickness of more than 500- μm . In 2001, OPGaAs was successfully grown to thickness in excess of 500- μm and characterized (Pinguet and others, 2001:138). The fabrication process of OPGaAs is summarized in Figure 3 (Eyes and others, 1998:276).

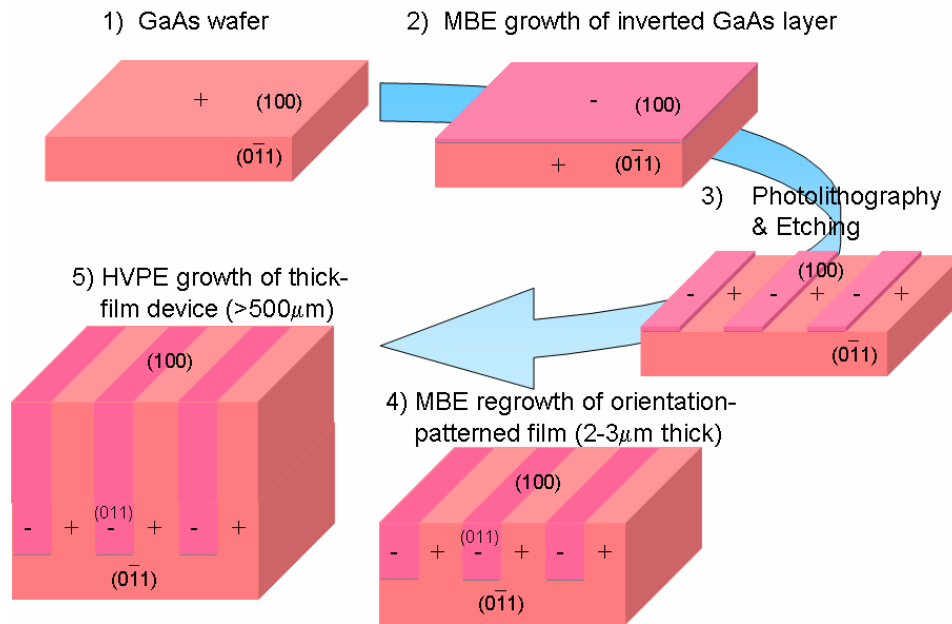


Figure 3: OPGaAs growth process

While the requirement for 1-mm thick OPGaAs samples in order to allow for larger pump beams has not been met, high quality samples over 0.5-mm are available. Increasing the thickness of OPGaAs is not without its challenges. The HVPE step uses hazardous gases such as arsine and growth runs are limited due to build-up of parasitic material in the HVPE chamber. HVPE growth can be stopped and restarted to attempt an additional growth layer of 0.5-mm. This technique has not proved successful, because

even after cleaning and polishing the top surface, the regrowth material quickly loses domain fidelity. Degradation of domain fidelity is seen in Figure 4 on page 17. Without proper domain spacing, QPM becomes inefficient if not altogether impossible.

III. Experiments

1. OPGaAs Samples

Seven OPGaAs samples were available for testing. Table 2 lists physical dimensions of the samples, the domain sizes, and template fabricators. The periodicity of the samples ranged from 49- μm to 63.8- μm . The samples were provided to Air Force Research Lab Electro-Optics Branch, AFRL/SNJW by Northrop Grumman Corp. and BAE Systems under the CARMA cooperative research agreement. The template fabricators, Stanford and BAE Systems, used techniques similar to the techniques described in the previous section. All HVPE thick-layer growth was performed by Air Force Research Lab Electromagnetics Technology Division, AFRL/SNH, located at Hanscom AFB, Massachusetts. Samples were manufactured at different times under slightly different conditions as manufacturing techniques evolved and thicker growth of the patterned material was achieved.

Table 2: Description of OPGaAs samples.

Sample	Length (mm)	Width (mm)	Thickness* (mm)	Periodicity (μm)	Growth Date	Source of Template
1	5.72	3.89	1.05	62	20 May 04	Stanford
2	7.74	5.42	0.75	49	20 May 04	Stanford
3	13.69	3.84	1.14	49	27 May 04	Stanford
4	10.29	6.07	1.15	62	27 May 04	Stanford
5	16.0	12.4	1.71	62/63/63.8	08 Apr 04	BAE
6	16.0	12.4	1.23	62/63/63.8	18 May 04	BAE
7	17.0	15.0	1.05	61/63	26 May 05	BAE

*Thickness measurement includes the substrate and orientation patterned material.

Direct measurement of the domain lengths was possible only on sample 5 since it was cleaved and polished along the length of a patterned region. All other samples were cleaved along areas of the template that did not contain orientation patterning. Using a Zeiss microscope, sample 5 was seen to have a domain periodicity of $63.8\text{-}\mu\text{m} \pm 0.9\text{-}\mu\text{m}$. Figure 4 shows the measured length of multiple domains and the measured thickness. Periodicity is lost as the domains grow farther from the substrate as is seen in Figure 4. Pinguet and others attributed similar loss of domain structure farther from the substrate to defects in the template used in the MBE process (Pinguet and others, 2001:138).

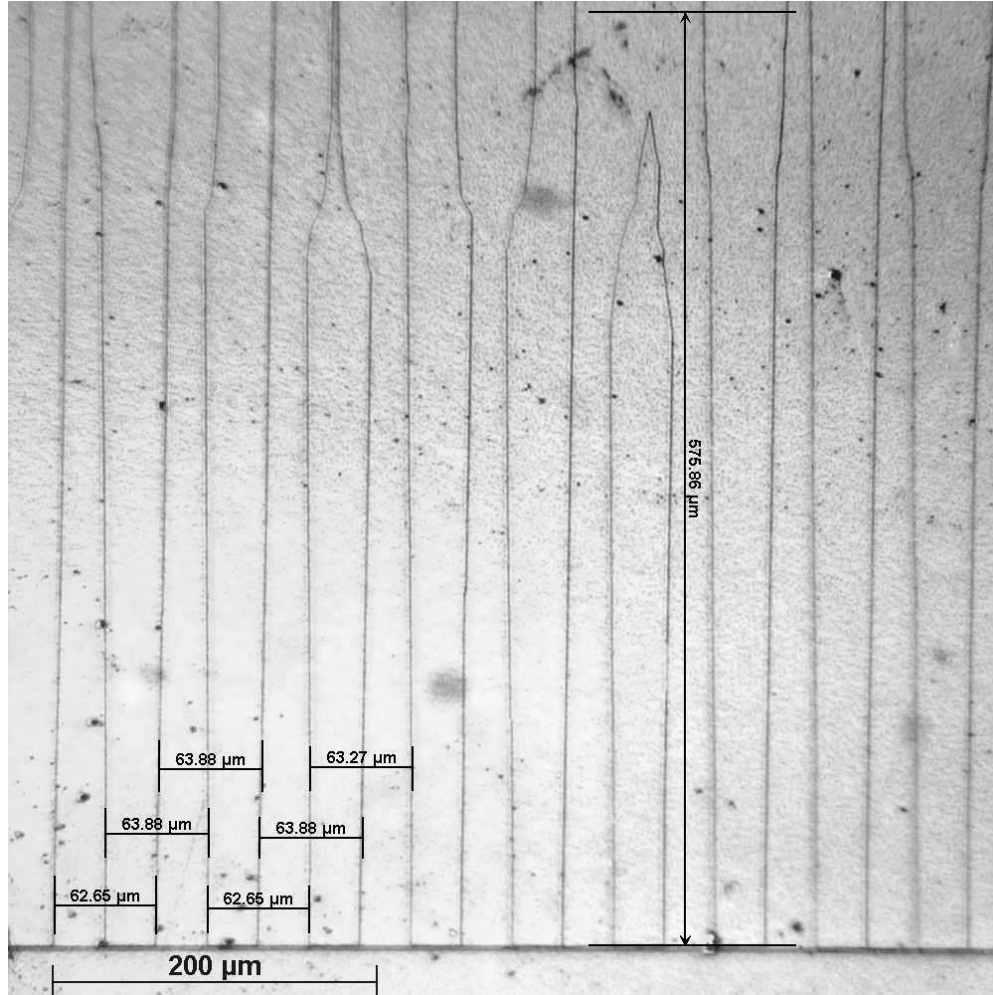


Figure 4: Magnified image of sample 6.

Sample vertical thickness was measured at 575.86- μm . Several domain regions are indicated with the shortest being 62.65- μm and longest being 63.88- μm . The designed length is 63.8- μm .

Thickness of the sample varies nominally across the width and along the interaction length. Direct measurement of the remaining samples was not possible without first cleaving the sample down the length of the crystal directly through a patterned region, a procedure with a high risk of causing permanent damage to the sample. Samples 5, 6, and 7 are more than twice as long and twice as wide as the other samples and were designed with multiple domains as can be seen in Figure 5.

The interaction length of each sample runs from top-to-bottom of the page. Left-to-right is the sample width. Also noticeable are the patterned and non-patterned areas. Samples 1, 2, 3, and 4 contain patterning across most of their area. Samples 5, 6, and 7 show large patterned areas separated by thin, non-patterned regions called streets. Streets are designed for ease of cleaving smaller crystals out of larger templates.

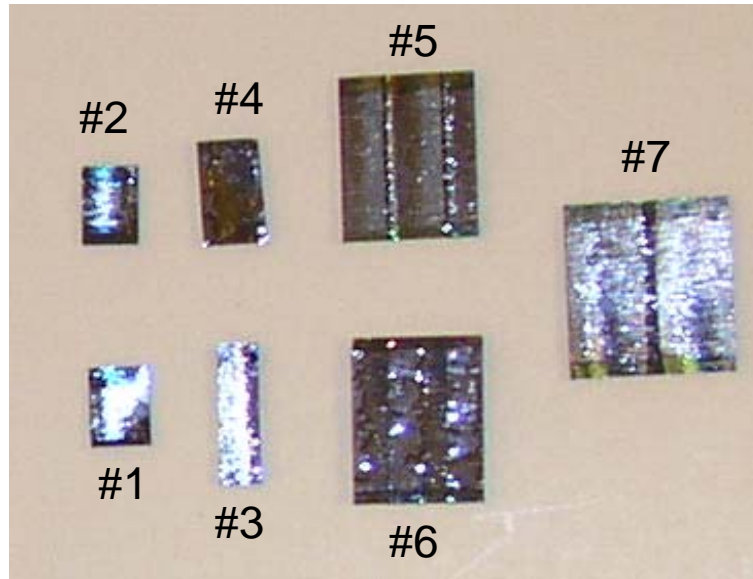


Figure 5: View of upper surfaces of samples.

Numbers refer to sample numbers used in this report.

Closer examination indicates most samples have some region of non-patterned material. Figure 6 shows sample 2 next to a ballpoint pen tip. Most of the area is patterned, while a prominent band along the left edge and faint band along the right edge are devoid of orientation patterns. The same is true of sample 6 seen in Figure 7. It contains a patterned region along the left edge allowing for the micrograph image captured in Figure 4. Alternating strips of non-patterned and patterned areas follow ending on the left, non-patterned edge. The patterned regions are variable in width along

the length. Figure 7 shows a patterned region in the center of the crystal containing a variable width along the length of the crystal (from top to bottom in the figure).



Figure 6: Sample 2 close up picture



Figure 7: Sample 6 close up picture

The input and exit faces of all samples are polished and parallel to each other. All samples were AR coated on the entrance and exit faces at the pump, idler, and signal wavelengths. Coatings on samples 1, 2, 3, and 4 were applied by Rocky Mountain Instruments while Quality Thin Films added coatings to samples 5, 6, and 7.

Figure 8 shows a representative graph of the percent of energy reflected from three samples 5, 6, and 7 as a function of wavelength. The coatings are designed to transmit near 100% of the signal and idler beams with a sacrifice of power lost to the pump beam.

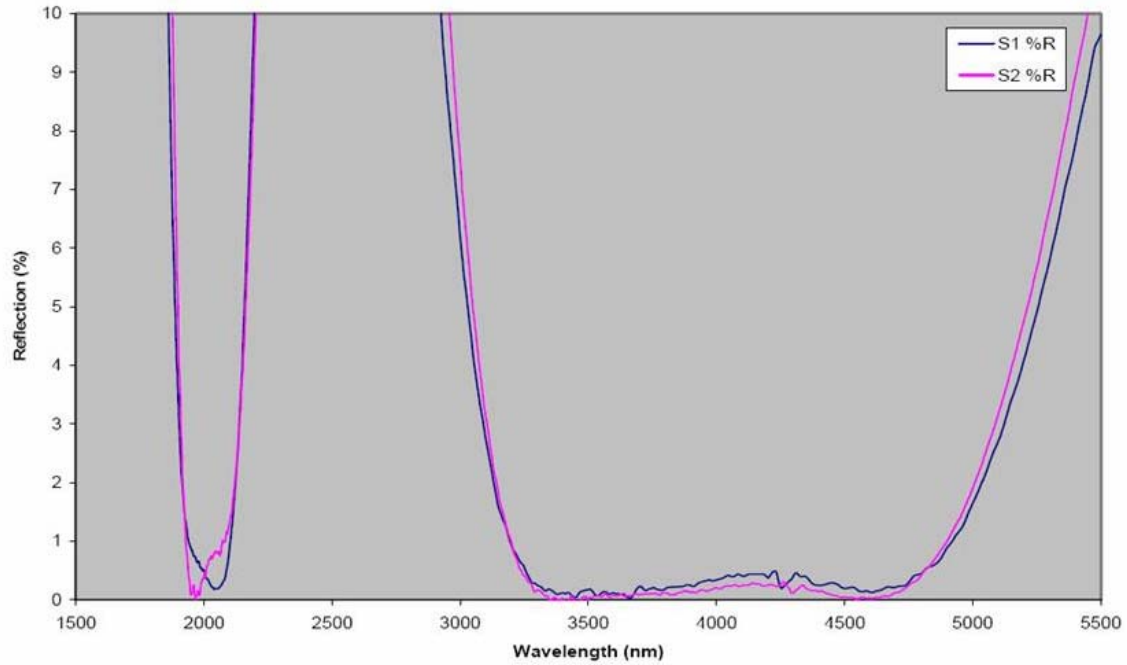


Figure 8: Sample coating performance plot.

A visual inspection of the coatings revealed unblemished surfaces across most of the area. Sample 4 did appear to have minor imperfections across the surface area of the input face.

2. *Pump Laser*

The pump laser was a laser-diode pumped, thulium-holmium-doped yttrium-lithium-fluoride (Tm,Ho:YLF) laser operating at 2.055- μm . The laser-diode was an Opto Power Corp. laser diode consisting of an array of aluminum gallium arsenide emitters operating continuous-wave (cw) at 0.792- μm . A closed-system water chiller extracted waste heat from the diode array. The laser diode output was delivered through a 1-meter optical

fiber. Output from the optical fiber was coupled into a Tm,Ho:YLF crystal using a pair of AR-coated 6-cm focal length lenses. The crystal was held in a copper cold finger in a liquid nitrogen-cooled dewar. The crystal was AR-coated for the pump and coated highly reflective (HR) for the laser on the side near the optical fiber. An acousto-optic Q-switch pulsed the pump laser at selected pulse rates from 100 Hz to 10 kHz. The Tm,Ho:YLF laser is a plano-convex cavity 20 cm in length with the HR coated side of the laser crystal acting as the planar end. The output coupler, a 1-meter radius of curvature (ROC) mirror, reflected 70% of the pump beam. The pump laser was capable of 2 watts average pump power in cw operation. The operating parameters of the Tm,Ho:YLF pump laser compared favorably to other similar reported experiments (Harm, 2002:22-25).

Attenuation of the intensity of the pump laser was achieved with the use of a half-wave plate and a polarizing Faraday isolator. The beam was focused using a 10-cm focal length lens AR coated for 2- μm . Figure 9 shows the pump laser test bed configuration used throughout the experiments.

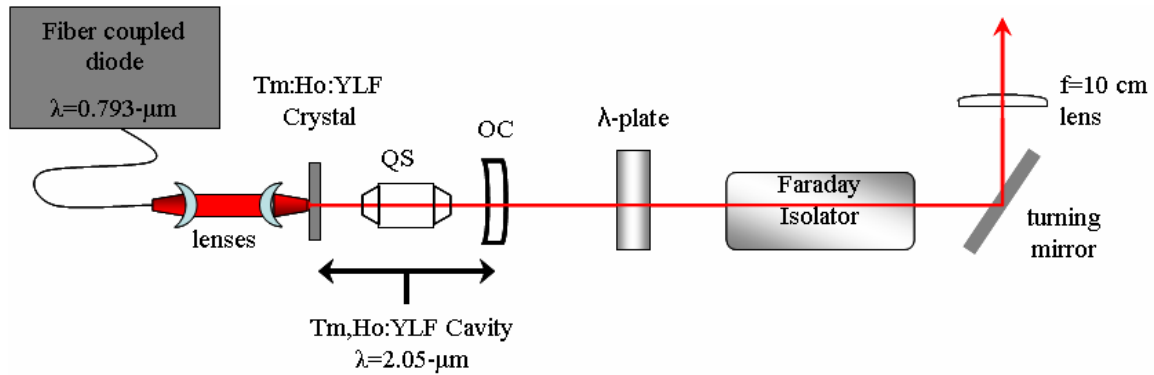


Figure 9: Tm,Ho:YLF pump laser

Paraxia modeling software was used to design a pump arrangement focused enough for reasonable conversion without clipping at the sample input and output faces. Using a

Nanoscan beam profiler, by Photon Inc, the size of the beam was measured. Figure 10 indicates the focused $\frac{1}{e^2}$ pump beam radius as a function of distance from the focusing lens. The focused beam reached a minimum radius of 86- μm in the x-axis and 72- μm in the y-axis with both occurring at 13.6 cm from the 10-cm lens. OPGaAs samples were placed in the beam path such that the beam waist occurred in the middle of the crystal. Figure 11 portrays the quality of the pump beam attenuated to power levels less than 5 mW when recorded by an uncooled, ferroelectric Electrophysics IR camera. The cause of the narrow fringes visible in Figure 11 is not known. They may be caused by aberrations induced by the various lens and mirrors. The Tm,Ho:YLF cavity, when pumped with 8 W to 15W of diode power, produces a clean, stable and reproducible beam as recorded by the camera over many hours of operation. An M^2 value of 1.3 was calculated for the pump train when operated at an average power of 80 mW.

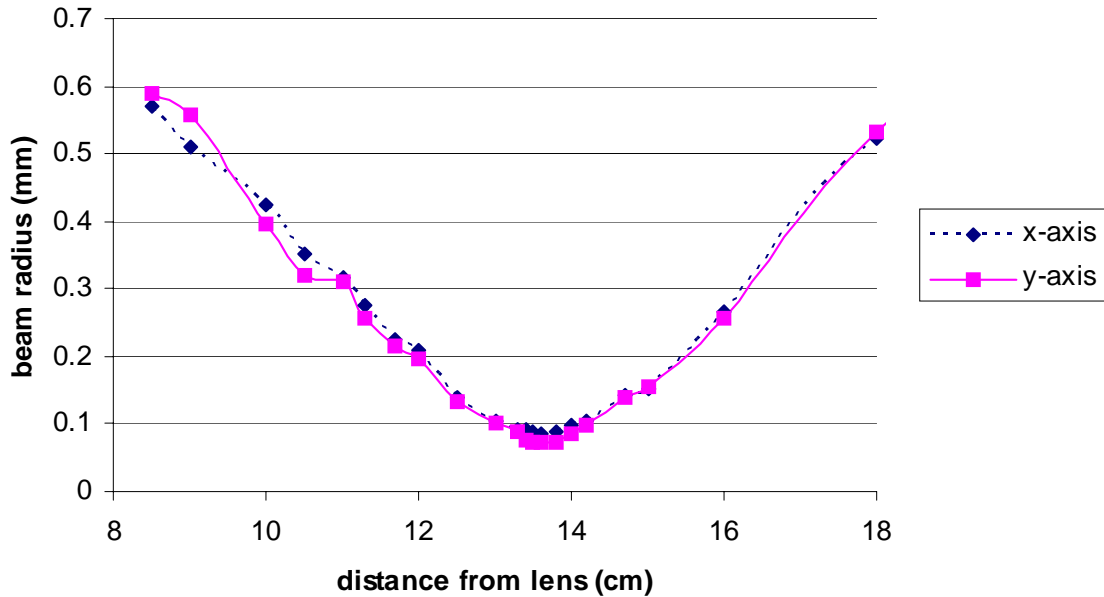


Figure 10: Pump laser beam waist profile.

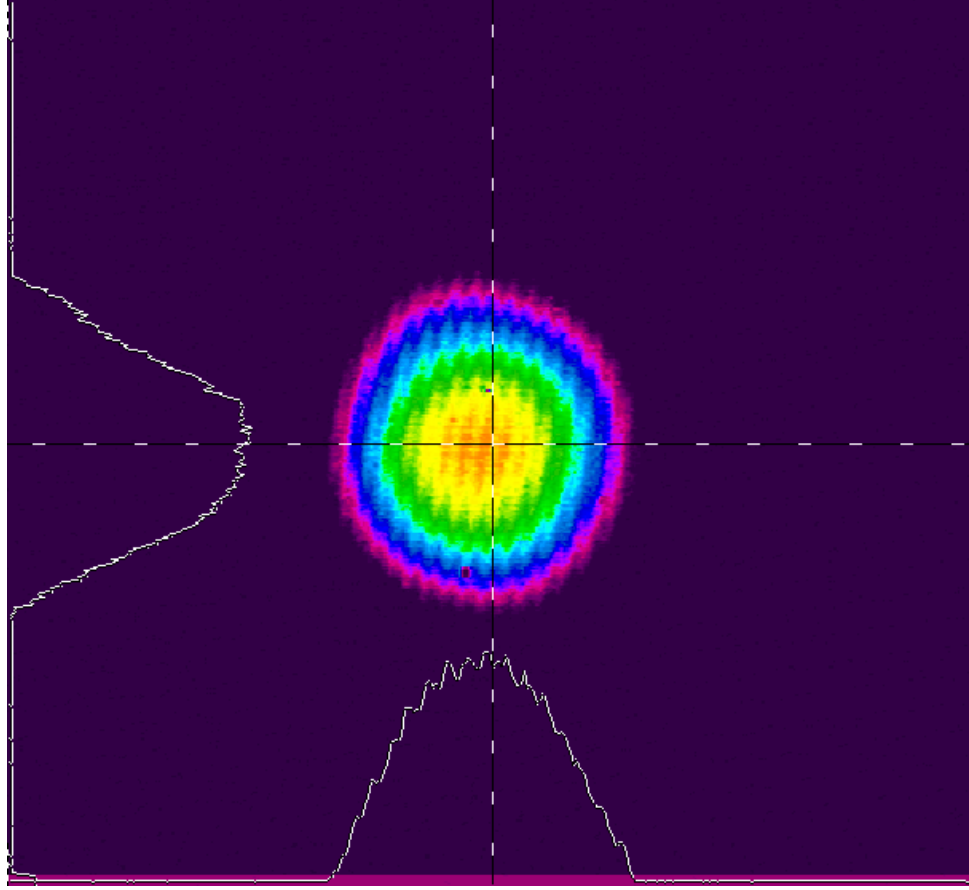


Figure 11: Pump beam intensity profile.

3. *Power Transmission Experiment*

Power transmission measurements were taken in a systematic manner to accurately calculate and describe transmission rates throughout the volume of the OPGaAs grown above the substrate. Samples were placed on an x-y translation stage. The stage also allowed for tip-tilt control for further alignment. The stage assembly was positioned so the minimum beam waist occurred approximately in the middle of the length of the crystal.

The OPGaAs samples were lightly secured to a stage with double-sided tape. No active measures were taken to cool the samples because the power levels were

significantly under coating damage threshold levels of 0.6 joules per square centimeter (Harm, 2002:26). Alignment of the crystal was performed to ensure propagation parallel to the length of each crystal thus preventing total internal reflections (TIR) off of the top and bottom surfaces. A propagating beam undergoing TIR was recognized because the intensity pattern moved quickly across the camera's field of view when the tip-tilt controls of the stage were slightly adjusted.

After alignment of the crystal, the Electrophysics camera was used to locate a corner of the crystal. The technique involved moving the x-y axis stage until it was evident the beam was no longer propagating through the crystal. This was evident because the image recorded by the camera was not changing despite translating the sample. The sample was slowly elevated up into the beam. The camera quickly recorded the aberrations caused by the crystal when the beam was clipping it. The elevation height was recorded and the sample was raised another 200- μm . The same procedure was used to find an outside edge of the crystal. Completion of this technique left the beam propagating approximately 200- μm below and 200- μm inside a corner of the crystal.

To record input power, a Newport optical power meter was placed 6 cm in front of the crystal face. Output power was measured at 6 cm beyond the crystal. A time delay of less than 30 seconds occurred between the measurements of the input power and output power due to physically repositioning the power detector. After the two power levels were recorded, the sample was translated. The process of recording the power readings was repeated until the entire surface of the crystal face was covered. The pattern resulting from the multiple measurements covered much of the input surface resembling the pattern shown in Figure 12.

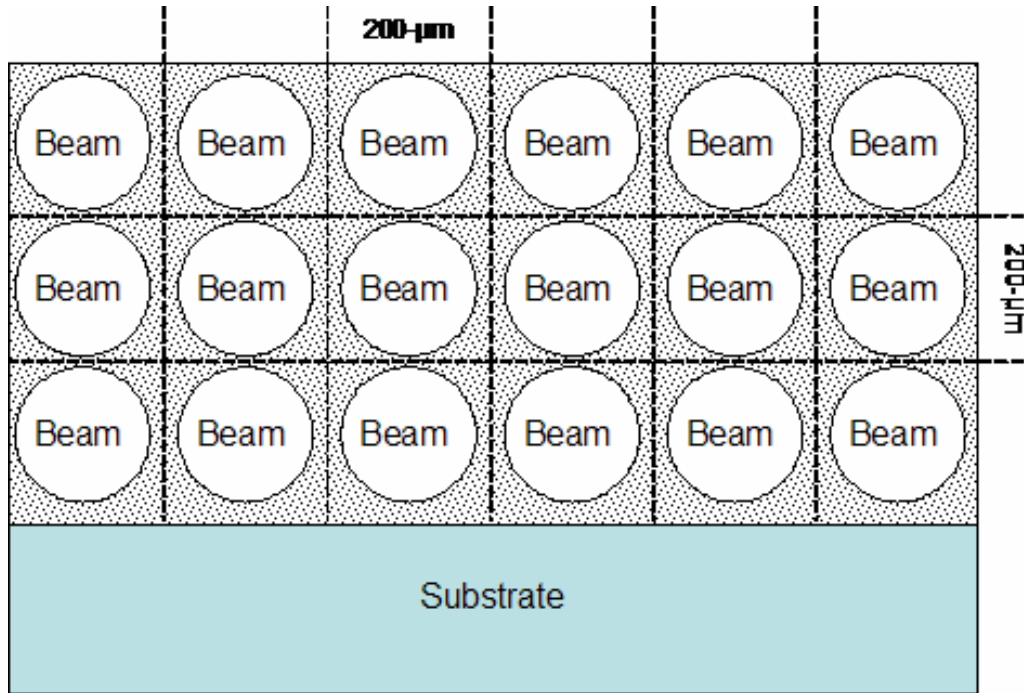


Figure 12: Depiction of pump beam probe pattern along face of OPGaAs samples.

Various levels of input power were used for this experiment ranging from 70 mW to 150 mW. Due to the size differences among the samples, the number of areas examined per sample varied. Sample 3 was tested in 62 locations while sample 7 was large enough for 204 unique paired input/output measurements. The mean number of paired measurements per sample was 130. A qualitative examination of the beam propagation is presented in the Appendix. It contains two representative sets of nine images taken at various locations in two samples.

4. *Scattering Experiment*

Scattering measurements were made by an indium gallium arsenide (InGaAs) photodiode detector mounted to an integrating sphere. A diagram of the complete scattering measurement test bed is shown in Figure 13.

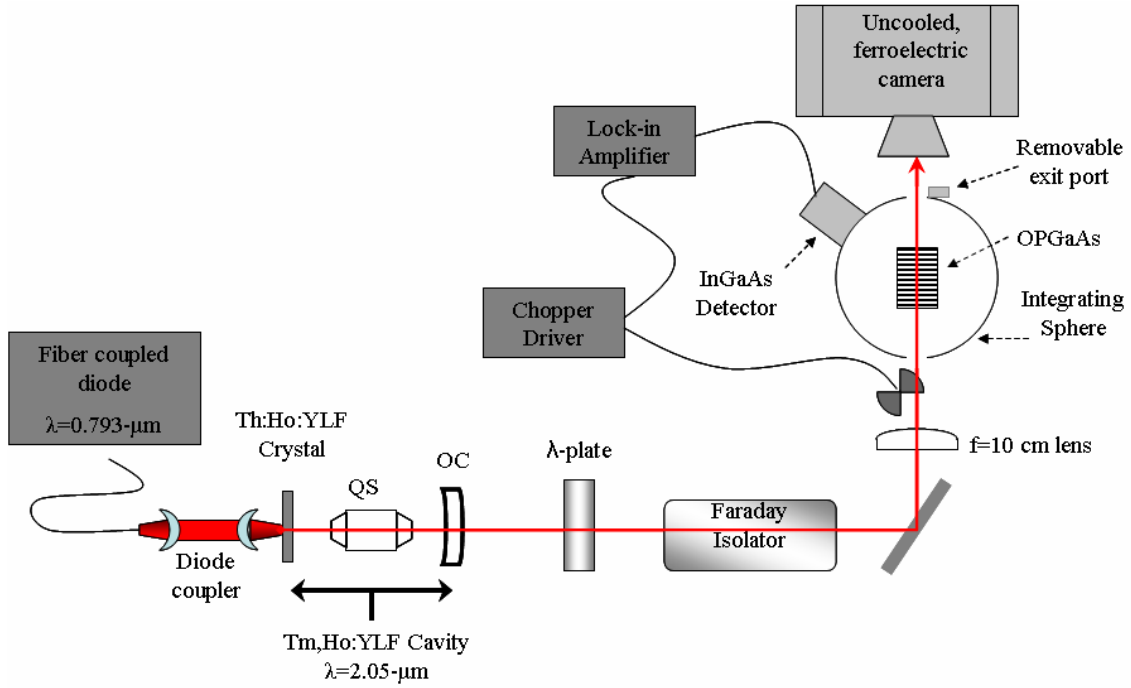


Figure 13: Scattering measurement setup.

Integrating Sphere: An integrating sphere was used to collect energy scattered as the pump laser propagated through various regions of each sample. An integrating sphere surrounds the sample and directs all scattered energy to a common location for measurement. In general, the sphere has at least two ports; an entrance port and a port for a detector. Additional ports may be available to allow for extra measurement devices.

The integrating sphere consisted of two aluminum hemispheres bolted together. The interior of the sphere was empty aside from two features. First, a post extended to the center of the sphere in order to support the OPGaAs sample. Second, a baffle was placed to shield the detector from receiving radiation scattered directly from the sample. Radiation was reflected from the diffuse coating until it reached the detector via an indirect route. The interior of the sphere was coated with barium oxide, a highly reflective diffuse material. The sphere had a removable port to allow the direct

transmission of the laser, but it was left on for the experiment. OPGaAs samples were placed on the sample holder, which allowed movement relative to the integrating sphere. The OPGaAs crystal was positioned so the minimum beam waist occurred in the middle of the length of the crystal. The entire sphere and sample-holder assembly were translated along the vertical and horizontal axes with micrometer precision. A Stanford Research Systems lock-in amplifier was used to reduce background noise readings. A mechanical chopper, operating at 77 Hz provided a reference signal for the lock-in amplifier. A close-up photo of the exterior of the integrating sphere assembly is shown in Figure 14 and the interior is pictured in Figure 15.

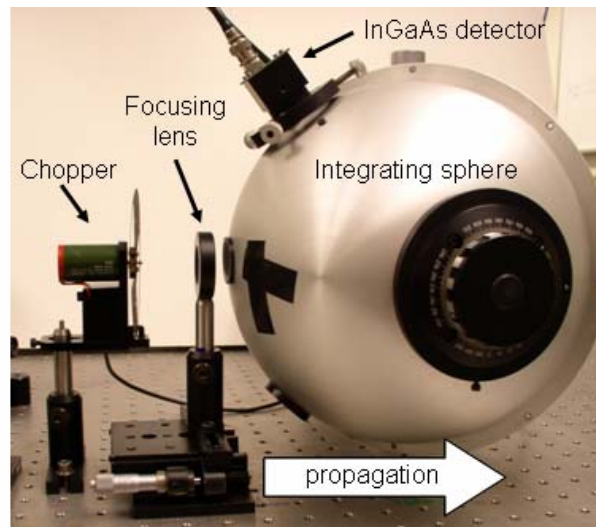


Figure 14: Photograph of integrating sphere assembly.

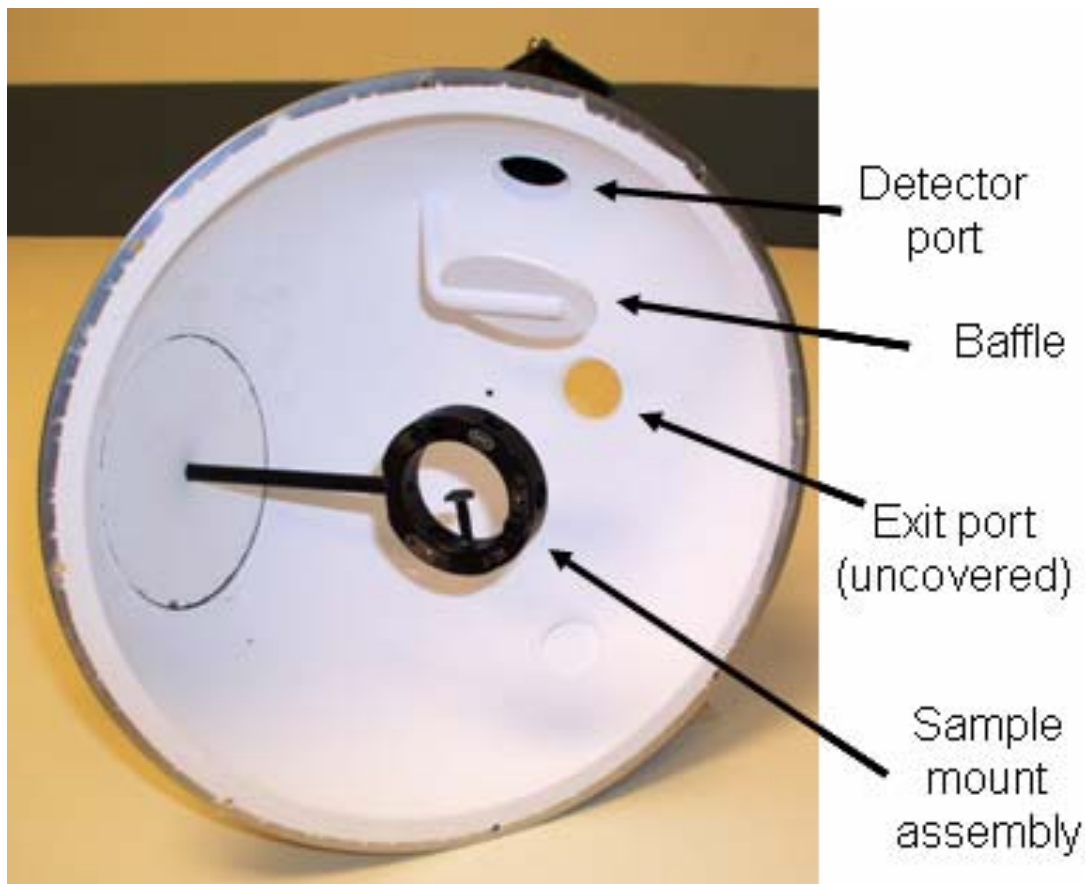


Figure 15: Integrating sphere interior detail.

Before samples were tested, the integrating sphere, detector and sample mount assembly were tested for uniform response as a function of position to ensure that changing the position of the sphere in relation to the beam did not introduce changes in the detected signal. The exit port was closed for these measurements. The beam impinged on the rear port cover and was not directly incident on the sample holder. Input power levels and detector response were recorded at each unique location.

Additional calibration of the integrating sphere was required for each sample to account for unique losses introduced by each sample. This loss, called indirect absorption occurs when a sample absorbs diffuse energy reflected from the inner walls of

the sphere. With the exit port covered and laser output attenuated to $99\pm0.5\text{mW}$, the beam was directed into the sphere striking the exit cover port. The sample was placed in the sphere and intentionally misaligned so none of the beam directly impinged on the sample or the sample holder.

Finally, scattering measurements were recorded. With the exit port of the integrating sphere removed to allow the use of the camera, alignment of a sample was performed exactly as indicated in the previous experiment. Once aligned, the exit port was replaced. The entire integrating sphere, detector, and sample were simultaneously translated to measure scattering through the same unique volume of material as before in the power transmission experiment. Average input power was measured before each scattering recording.

5. *Reflection Experiment*

Power reflection from the front face of each sample was required for a complete analysis of the loss mechanisms in each sample. Although the samples were AR coated, the coating was maximized at the signal and idler wavelengths. The crystal was placed such that the middle was located near the beam's minimum waist and fine-tuned with a tip-tilt stage. The crystal face was grossly aligned perpendicular to the beam. Starting with low power settings of around 5 mW, crystal face was turned about 3 degrees off center, just enough to allow for measurement of the reflected beam without obstructing the pump beam. The camera was used to ensure that only the reflection from the front face was being recorded and that rear faces reflections were not in the field of view. With the alignment confirmed, the camera was replaced with the power meter and input

power increased to approximately 200 mW. Reflected power was measured from multiple surface positions on the front face of each sample.

6. *OPO Experiment*

Using the pump assembly described earlier, a singly resonant, linear OPO cavity was constructed. An SRO design was attempted because of available mirrors with appropriate coatings and the fact an SRO cavity is usually easier to align as compared to a doubly-resonant cavity since the tolerance to mode-match one resonating beam is much greater than the range of acceptable values that simultaneously matches two resonating frequencies. Two, calcium fluoride (CaF_2) meniscus mirrors coated to pass the idler and pump beams and reflect 99.99% of the signal beam at 3.6- μm , formed the cavity. They measured 1-inch by 0.25-inch with a ROC of 5 cm and were positioned equal distances from the faces of the OPGaAs and mounted in micro-adjustable lens holders resulting in a confocal resonator. The length of the OPO cavity was 6.8 cm with the center of the cavity at the beam waist. Output from the OPO was filtered using a 3- μm long-pass filter with a transmission range of 3.073- μm to 8.319- μm . In addition, a graduated neutral density filter was used whenever pump output was suspected of exceeding camera tolerances. Figure 16 shows the completed OPO cavity set up.

Sample 7 was incorporated in the OPO experiment since preliminary results from the scattering and absorption measurements indicated it had the lowest loss coefficients, it was a wide sample allowing for easier alignment, and the domains were of the correct length for phase matching.

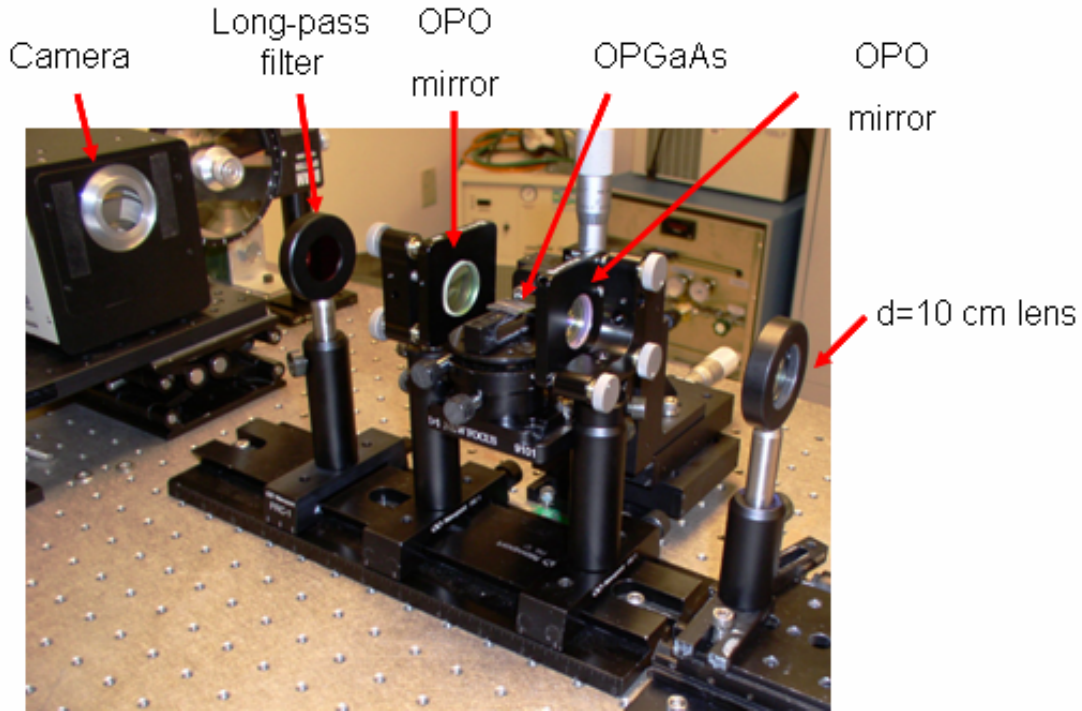


Figure 16: Tm,Ho:YLF pumped OPO cavity

Alignment of the OPGaAs sample was accomplished with the OPO mirrors removed. The faces of the sample were perpendicular to the pump beam. The sample was positioned with the aid of the camera verifying a TIR phenomenon was not occurring. The sample stage was translated a known amount to position the beam in a region of the crystal exhibiting high power transmission qualities. The micrometer adjustments on the stage made it easy to lower the sample a known amount so the mirrors could be aligned then elevated back into the same position.

Several techniques were employed to align the cavity mirrors. The technique involved aligning from downstream-to-upstream. With the input OPO mirror removed and the sample holder empty, the output OPO mirror was adjusted so the reflected pump returned back onto itself. Liquid crystal paper sensitive to temperature was used to locate

the reflected beam. Finding the exact position of reflected beam became impossible once it overlapped the pump beam.

Next, the input OPO mirror was installed with the curvature of the mirror reversed compared to the final operation in order to keep the reflected beam focused back upstream. The input mirror was adjusted so the vertical travel of the reflected beam was at the same height at the pump beam. The input mirror was turned 180 degrees for final alignment. Raster scanning the input mirror became the technique for final alignment.

IV. Data and Analysis

1. Reflection Losses

The amount of power lost due to reflection was measured with the sample input face near-normal to the beam since the coating on the samples does not transmit 100% of the pump beam. Since the transmission amount is also angle dependent and a maximum at normal incidence, measurements were taken with the sample as close to normal to the pump beam as possible. The data taken from each sample are summarized in Table 3 with the calculated reflection coefficient indicated.

Table 3: Measured reflection coefficients of all samples.

Sample	Input Power (mW)	Reflected Power (mW)	Reflection Coefficient
1	223	27.04	0.10
2	210	4.01	0.02
3	205	2.97	0.016
4	205	2.53	0.014
5	204	1.86	0.049
6	205	9.02	0.01
7	205	4.11	0.03

2. Scattering and Absorption Losses

Since the interior of the sphere is not perfectly diffuse and some inherent absorption occurs, a simple calibration measurement of the sphere was performed. To account for the minimal amount of absorptive material in the sphere affecting the outcome of every

scattering measurement, a series of measurements were taken without any sample in the sphere and the exit port covered. The sphere was translated through the entire range of movement. The input power was 86 ± 0.5 mW for each of 136 readings. The average reading was 12.42 mV with a standard deviation of 0.28 mV indicating the sphere was a uniform diffuser throughout the range of motion.

Measurements were taken without any samples in the sphere to determine the response of the detector. The InGaAs detector operated with almost near linear response in the limits of power used throughout the experiments. The response of the detector along with a linear fit of the data is shown in Figure 17. The linear fit shows the response was 6.0 plus 0.08 times the input power.

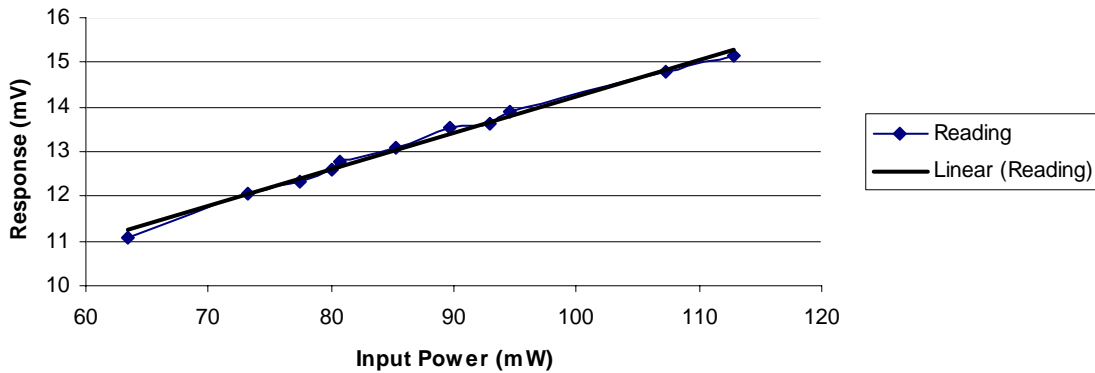


Figure 17: InGaAs detector response.

Indirect absorption is defined as energy lost when sample absorbs diffuse energy reflected from the inner walls of the sphere. The recorded amounts of indirect absorption at 99 mW input power are listed in Table 4.

Table 4: Indirect absorption per sample.

Sample	Detector Reading (mV)	Indirect Loss (mV)	Percent Loss
1	13.68	0.48	3.5
2	14.04	0.12	0.9
3	14.07	0.08	0.6
4	14.09	0.07	0.6
5	13.99	0.17	1.2
6	14.08	0.08	0.6
7	14.03	0.12	0.9

The use of an integrating sphere to distinguish loss behavior has been around for many decades. An outline of the equations shown below follows a classic approach detailed in other sources (Bastin and others, 1959:412-414). Required measurements include finding the average beam power propagating into a crystal, I_o , and measuring the corresponding average power exiting a sample, I_T . This yields the required ratio of $\frac{I_T}{I_o}$.

The next pair of measurements includes placing the sample in the integrating sphere as described in the Integrating Sphere section beginning on page 27 and recording the total amount of indirect absorption, I'_S , and the total amount of scattered plus transmitted energy, I_S . These two recordings give the ratio $\frac{I'_S}{I_S}$. A measurement of the total loss coefficient, Δ , through the sample due to both scattering and absorption is calculated

from (9) where I_T is the transmitted intensity measured in units of power, I_O is the original input intensity measured in units of power, R is the percent of power reflected normal to the perpendicular face of the sample. The distance of propagation, d , is the length of the OPGaAs crystal.

$$\frac{I_T}{I_O} = \frac{(1-R)^2 e^{-\Delta d}}{1-R^2 e^{-2\Delta d}} \quad (9)$$

The absorption loss coefficient, α , is found from (10) assuming a single photon has a negligible chance of undergoing both scattering and absorption. In other words, the two processes of scattering and absorption are considered to be independent. The voltage measured by the photodiode when the laser impinges on the sample, I_s , is compared to the photodiode measurement, I'_s taken with the sample in the sphere and displaced out of the laser beam.

$$\frac{I_s}{I'_s} = \frac{R - R^2 e^{-\alpha d} + (1-R)^2 e^{-\alpha d}}{1 - R e^{-\alpha d}} \quad (10)$$

Equations 9 and 10 are solved for Δ and α , respectively. The amount of scattering, σ , is calculated from (11).

$$\sigma = \Delta - \alpha \quad (11)$$

Calculated absorption, scattering, and total loss coefficients are shown in Figures 18 through 24. The three plots on each page indicate data collected from each sample in a manner indicated by Figure 12. Each figure displays the three sets of data starting on top with the measurement taken with the probe beam centered on 480- μm from the substrate. The remaining two charts per figure show the measurements taken at distances from the substrate of 280- μm and 80- μm . The vertical scale remains unchanged except on the plots in figures 22, 23, and 24. A scaled diagram of the input face is included under the lower plot of each figure since the areas of patterning are areas of interest. As noted on the top of page 20, the width of the patterned regions is variable along the length of the crystal resulting in ‘edge effects’. The edge between a patterned and non-patterned region is sharply depicted in the scaled drawings, not fully consistent with reality as shown in Figure 7. Edge effects are seen in many of the subsequent plots by a gradual increase or decrease in the loss coefficient, rather than abrupt change, when comparing adjoining patterned and non-patterned regions. The scaled diagrams show (1) the substrate, indicated by uniform, gray coloring, (2) patterned regions shown in cross-hatched areas, and (3) and solid, white, non-patterned areas.

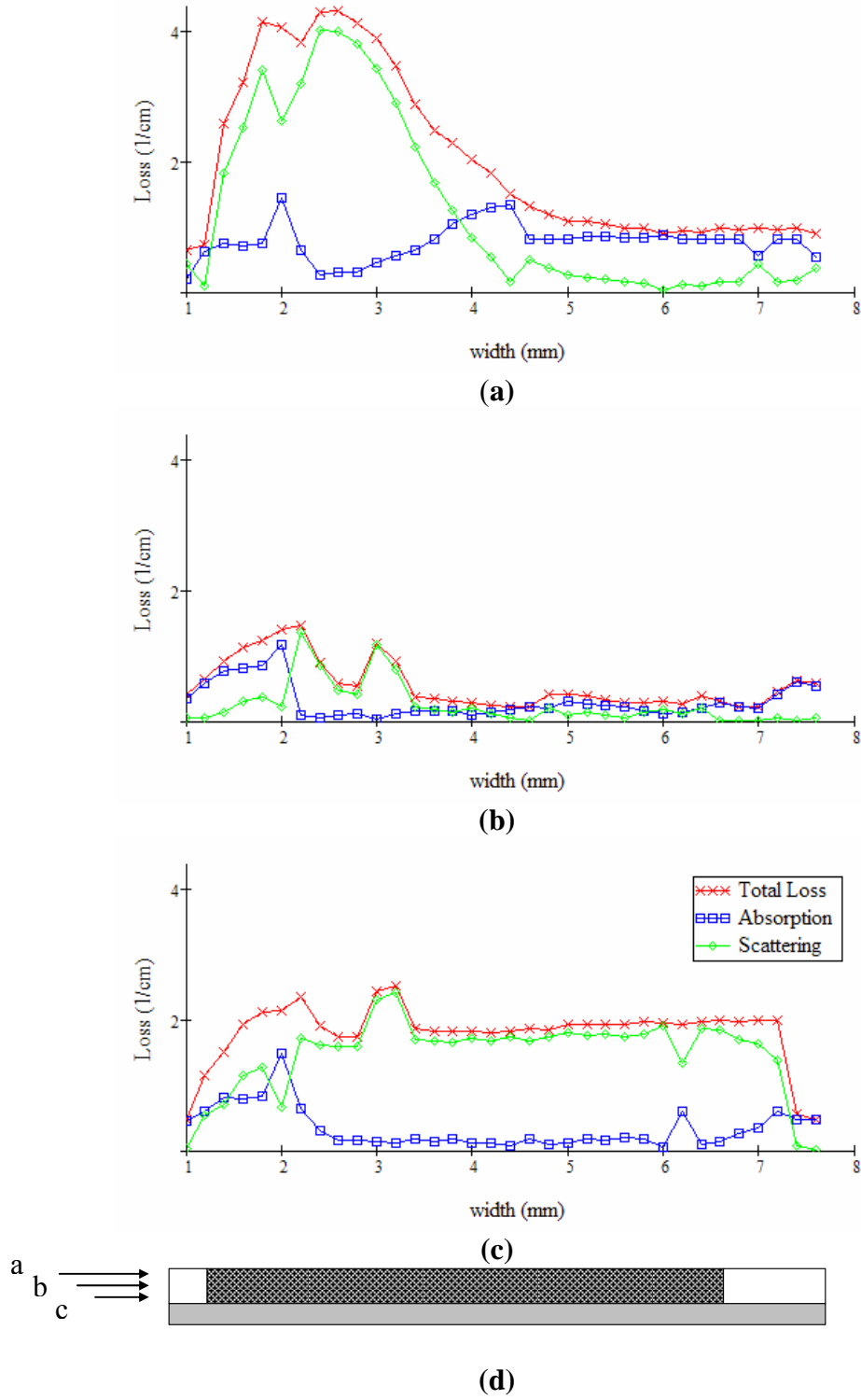
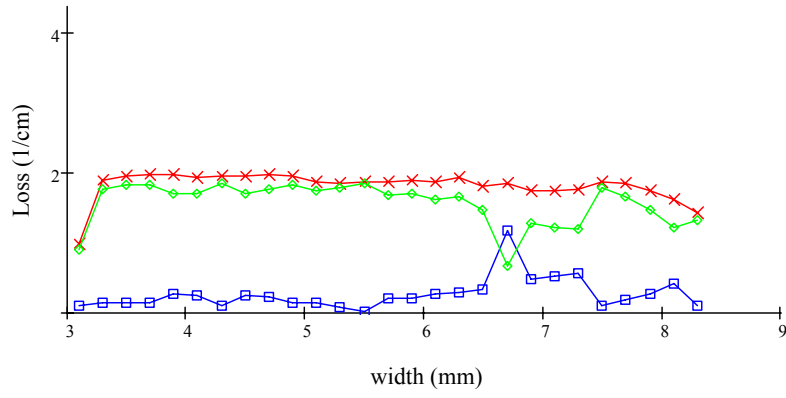
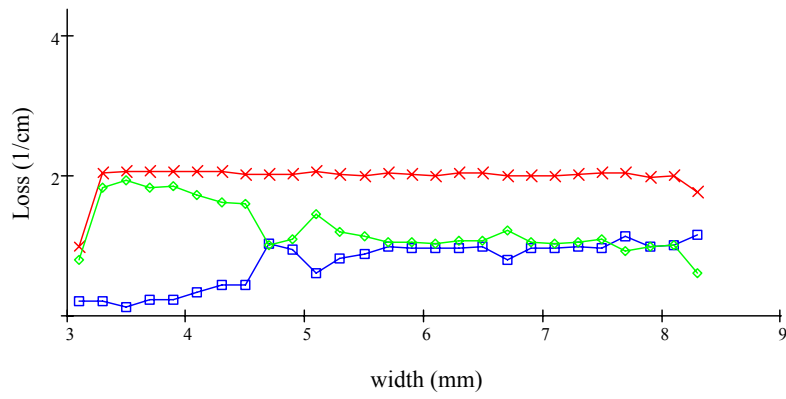


Figure 18: Sample 1 losses.

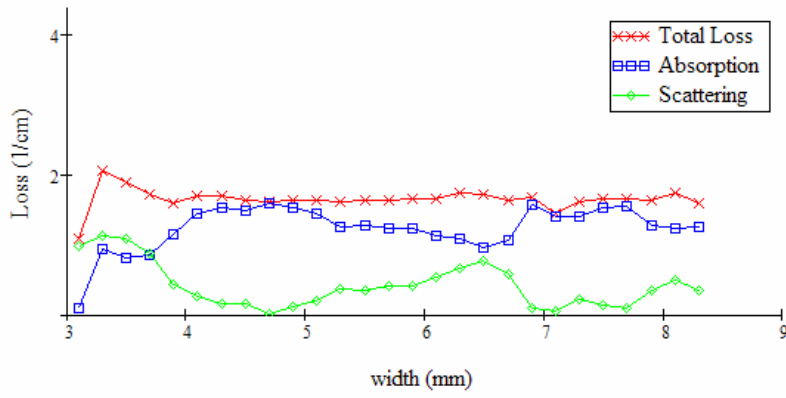
(a) 480-μm from substrate, (b) 280-μm from substrate (c) 80-μm from substrate and (d) scaled end-view of sample depicting patterned areas and non-patterned areas.



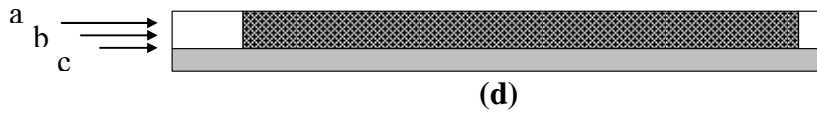
(a)



(b)



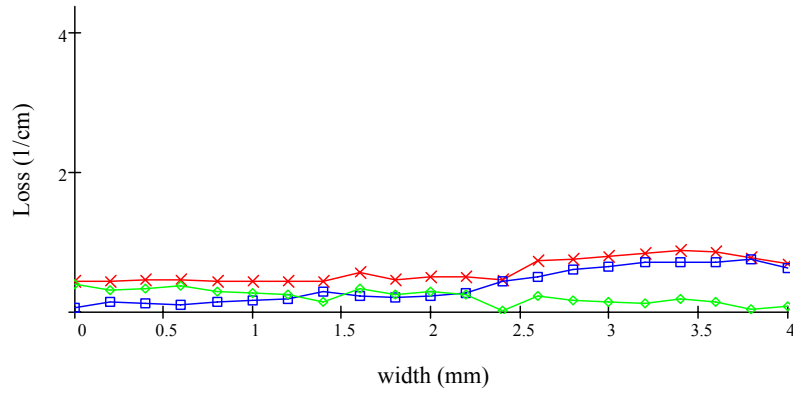
(c)



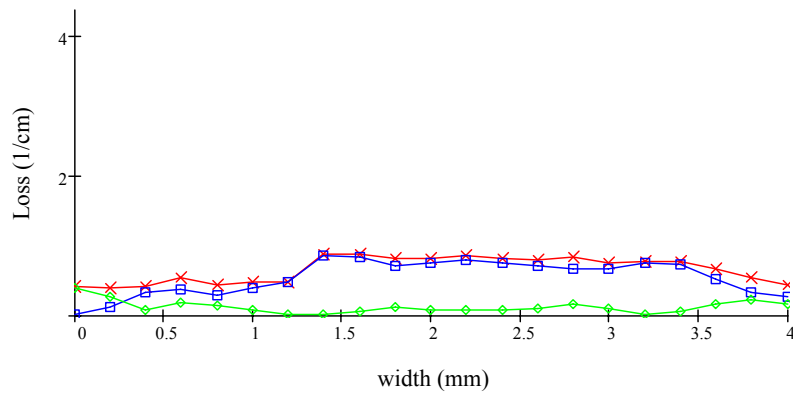
(d)

Figure 19: Sample 2 losses.

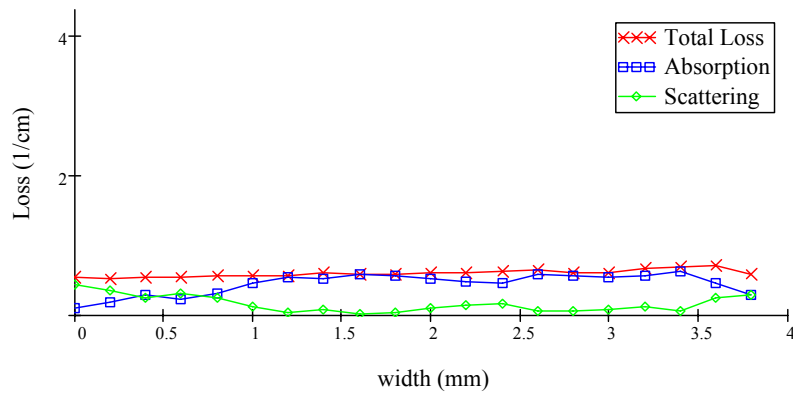
(a) 480-μm from substrate, (b) 280-μm from substrate (c) 80-μm from substrate and (d) scaled end-view of sample depicting patterned areas and non-patterned areas.



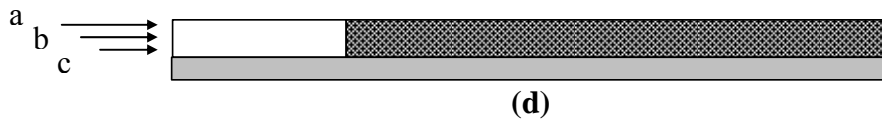
(a)



(b)



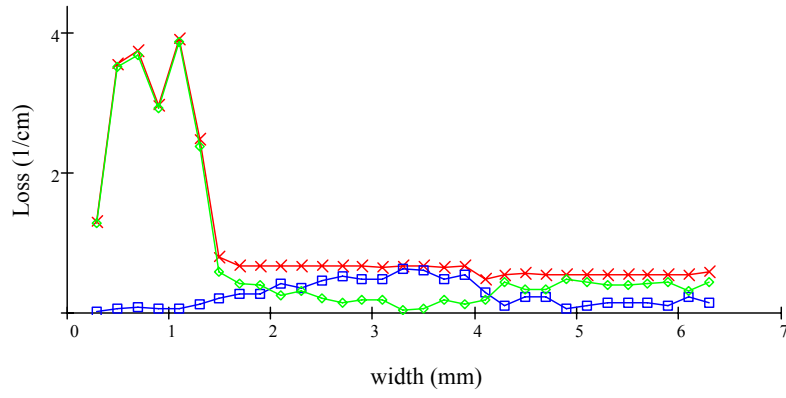
(c)



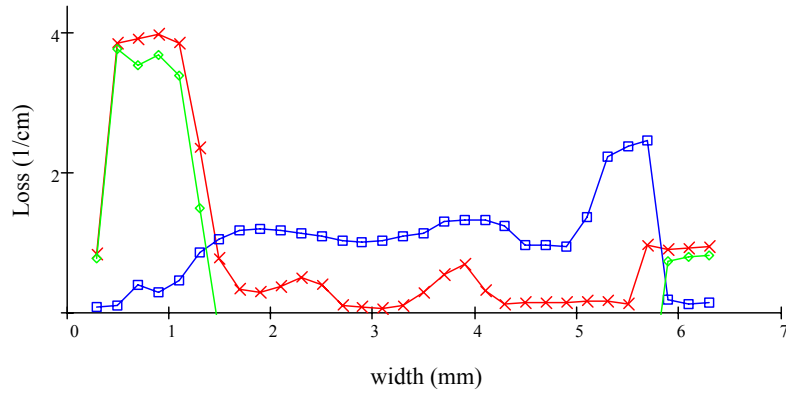
(d)

Figure 20: Sample 3 losses.

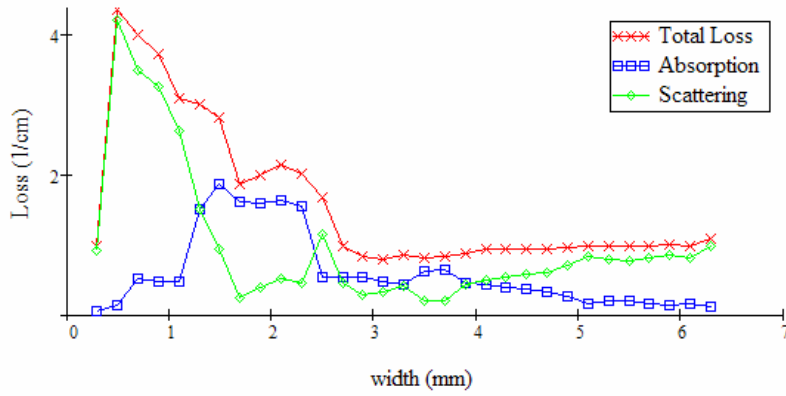
(a) 480- μm from substrate, (b) 280- μm from substrate (c) 80- μm from substrate and (d) scaled end-view of sample depicting patterned areas and non-patterned areas.



(a)



(b)



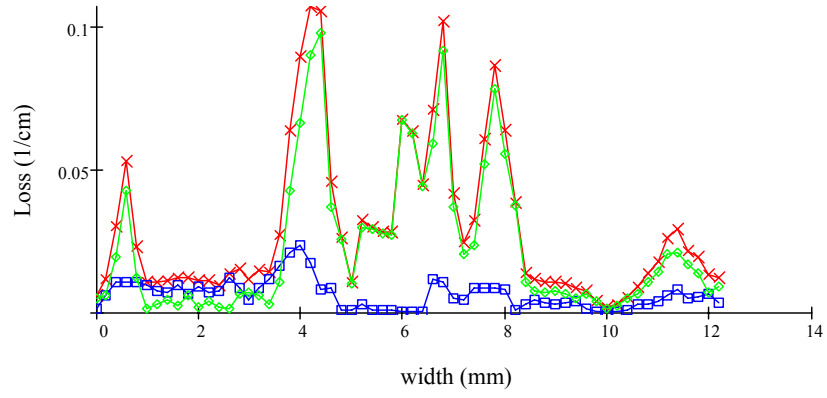
(c)



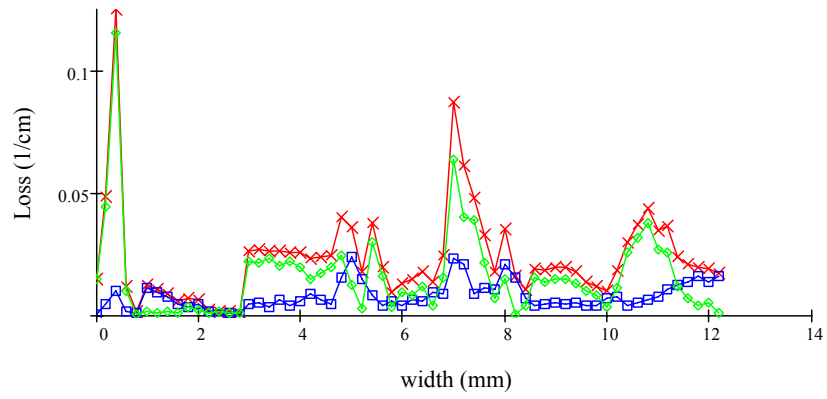
(d)

Figure 21: Sample 4 losses.

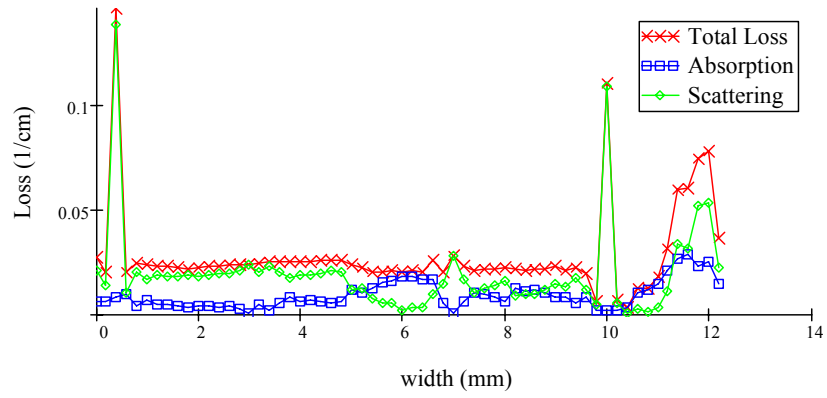
(a) 480- μm from substrate, (b) 280- μm from substrate (c) 80- μm from substrate and (d) scaled end-view of sample depicting patterned areas and non-patterned areas.



(a)



(b)



(c)



(d)

Figure 22: Sample 5 losses.

(a) 480- μm from substrate, (b) 280- μm from substrate (c) 80- μm from substrate and (d) scaled end-view of sample depicting patterned areas and non-patterned areas.

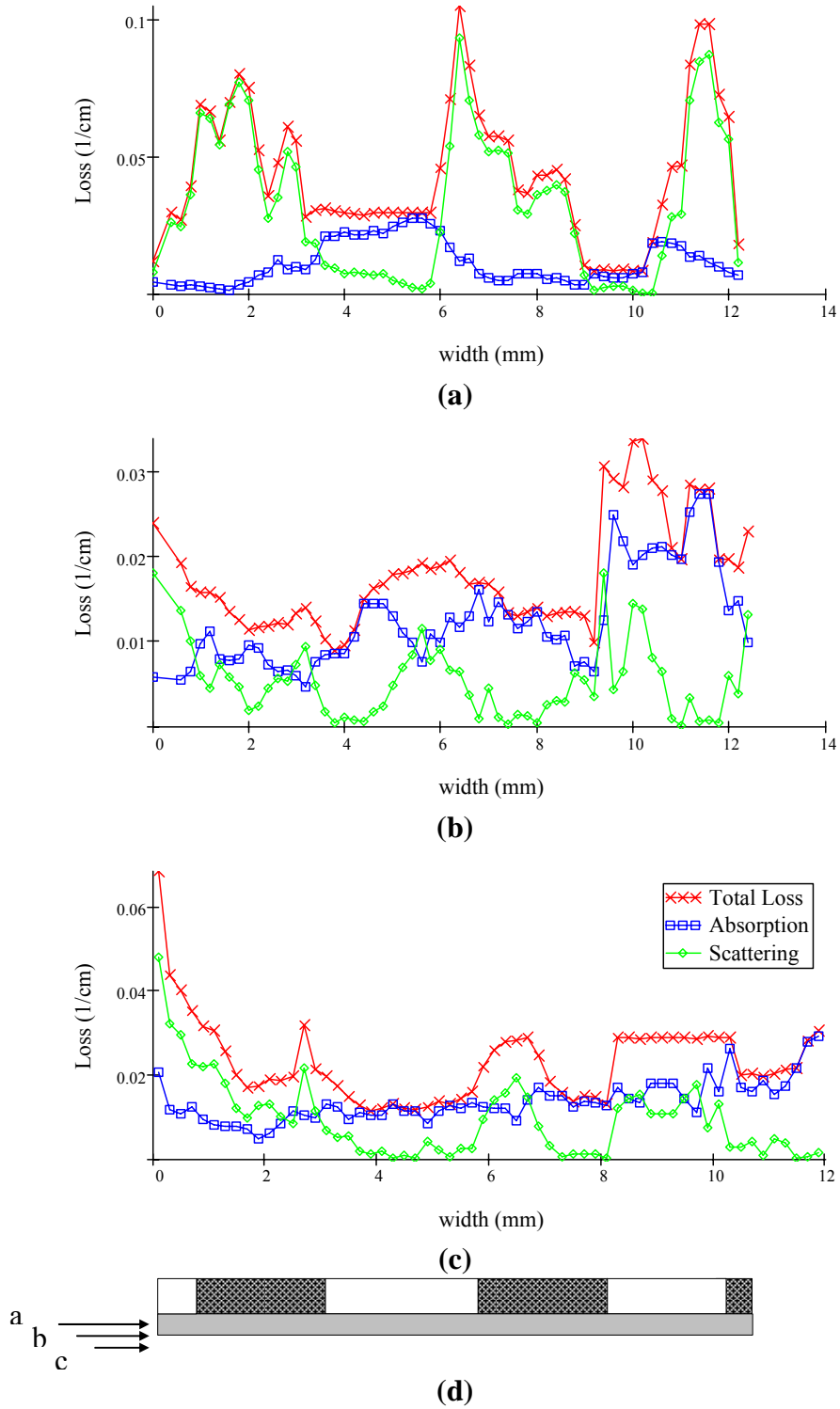
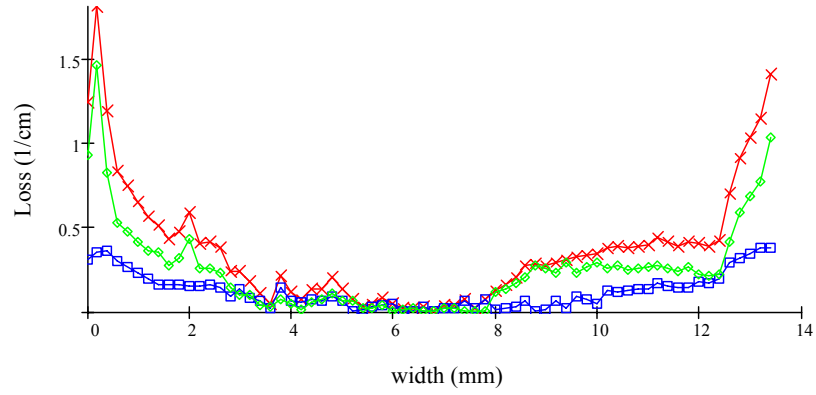
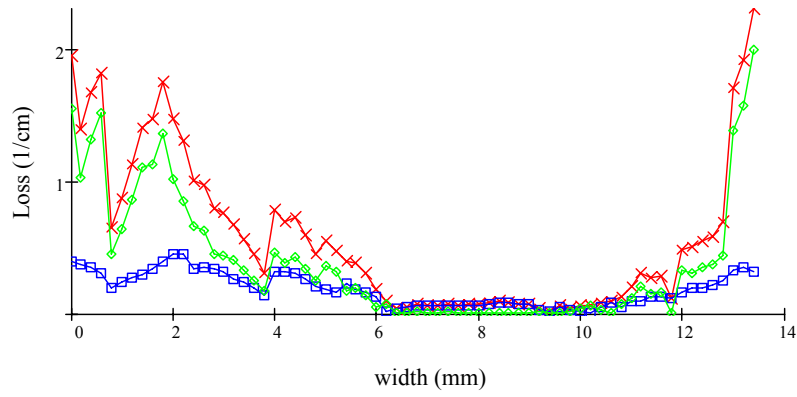


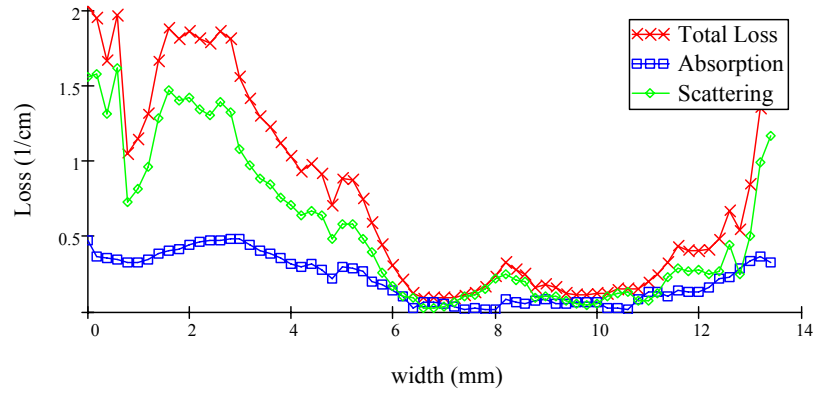
Figure 23: Sample 6 losses.
(a) 480- μm from substrate, (b) 280- μm from substrate (c) 80- μm from substrate and (d) end-view of sample depicting relative patterned areas and non-patterned areas.



(a)



(b)



(c)



(d)

Figure 24: Sample 7 losses.

(a) 480- μm from substrate, (b) 280- μm from substrate (c) 80- μm from substrate and (d) end-view of sample depicting relative patterned areas and non-patterned areas.

A summary of the data is depicted in Table 5. The average indicated is that of all the data taken for each sample. The standard deviation of the data set is listed beside each average value. The data set includes all patterned and non-patterned regions in each sample.

Table 5: Loss coefficients summary

Sample	Average Total Loss Coefficient (1/cm)	Standard Deviation	Average Absorption Coefficient (1/cm)	Standard Deviation	Average Scattering Coefficient (1/cm)	Standard Deviation
1	1.5	1.0	0.5	0.36	1.0	1.0
2	1.8	0.2	0.75	0.50	1.1	0.6
3	0.6	0.2	0.50	0.22	0.2	0.1
4	1.2	1.2	0.62	0.6	0.6	1.4
5	0.03	0.03	0.008	0.006	0.02	0.02
6	0.03	0.02	0.01	0.006	0.02	0.02
7	0.6	0.6	0.18	0.14	0.40	0.4

Scattering is the overall dominant loss mechanism in most samples. Samples 5, 6, and 7 grown on BAE templates, regardless of the date of manufacture, show on average more loss due to scattering than absorption. Of the four samples grown on Stanford templates, samples 1, 2, 3, and 4; the two oldest samples, 1 and 2, show on average more loss due to scattering while the two newer samples, 3 and 4, exhibit more absorption compared to total loss. The higher loss factors in the samples using Stanford templates

are counterbalanced by the overall consistency of the quality throughout the sample. Consistency is certainly an important factor in final implementation of OPGaAs into an operational military system. In contrast, samples on BAE templates indicate much higher optical quality at the expense of consistency. The OPO design considered in the report was controlled in a laboratory environment free of vibrations. This allows one to confidently choose the best location in the sample to pass the beam. In an operational system, it could be speculated that factors such as jitter and a required larger beam radius would cause the beam to pass through regions of the sample that are less desirable giving rise to an unpredictable OPO power.

Distance from the substrate does not seem to be a factor in determining the dominant loss factor. Figures 18 through 24 indicate various levels of scattering compared to absorption at different distances from the substrate. Sample 1 is dominated by scattering effects nearest the substrate with absorption and scattering about the same farther from the substrate. Sample 2 has high absorption nearest the substrate with scattering becoming the leading factor in farther from the substrate. Sample 3 has a large absorption coefficient throughout the entire crystal whereas sample 5 and sample 7 have scattering as the dominant loss term. Sample 6 has a larger absorption coefficient nearest the substrate, then a dominating scattering coefficient in the middle of the sample, and reverts back to a larger absorption coefficient farthest from the substrate. In conclusion, no correlation is apparent between the type of loss mechanism and the distance from the substrate. This observation may be of great importance since one might assume growing increasingly thicker samples will not decrease the quality of the samples. Thicker

samples have been grown at the expense of losing fidelity in the orientation patterning but the optical losses have not been measured in samples thicker than 600- μm .

Quality of the OPGaAs samples does appear to be influenced by their date of manufacturing. The two oldest samples, 5 and 6, have the lowest total loss coefficients. All samples used in this research produced since 18 May 2004 consistently have larger total loss coefficients. These results are contrary to the casual assumption that materials improve over time due to improved techniques and understanding. It should be noted that other causes may be negatively impacting the advancement of a material such as fluctuations in monetary investment levels over time, maintenance and down-time on one-of-a-kind machines used in the manufacturing of OPGaAs, and lower prioritization on research as newer, more exotic materials demonstrate even greater rewards.

Results of the samples on BAE templates confirm larger total loss coefficients in the patterned regions compared to the non-patterned regions. This result was initially anticipated since the patterned regions might be visualized as multiple interfaces similar to an older method of OPGaAs construction using fusion bonding. Multiple interfaces undoubtedly introduced reflection and scattering losses when compared to the same material void of interfaces. Conversely, the samples on Stanford templates show consistent loss values throughout most of the patterned regions.

3. *OPGaAs OPO*

Successful OPO operation proved elusive. The inability to obtain any output from the OPO using sample 7 was disappointing. Gain could not overcome inherent material losses in the samples, and attempts to obtain output led to coating damage and possible

damage to the crystal. The inability of the coating to withstand a fluence level above 1.5 joules per square cm is a limiting factor in sample 7. While the entire experience was educational no results were acquired for analysis and discussion. Yet, the experience was not in vain. The next section discusses several recommendations for future work with these samples in the hope of demonstrating an OPO with one of the samples.

V. Conclusions and Recommendations

1. Conclusions

It is not clear whether or not OPGaAs optical quality is improving with time. Results showed the two oldest samples have the least optical loss. Consistency of each sample in terms of total loss may be dependent on the manufacturing source. Most crystals grown on Stanford templates show slowly changing amounts of loss from one region of a crystal to another. All the crystals on BAE templates indicated relatively larger amounts of loss in the patterned regions compared to non-patterned regions.

2. Recommendations

Future work with these samples with the goal of designing a successful OPO is recommended. The coatings of samples 5 and 6 are undamaged leaving two good candidates for building a nonlinear device. The interaction length is the longest we have and should provide for high gain per pass. Sample 5 is especially promising since the overall loss coefficients were especially low.

The materials and equipment used in these experiments are in good condition. The collection of OPGaAs samples owned by AFRL/SNJW is the best known lot for comparisons of many different factors. Aside from damaging sample 7 in the OPO experiment, no other damage occurred. Due to the age of some of the samples and uncertainty on how they were stored, it is recommended damage inspections be done on samples 1, 2, 3, 4, and 6 on the coatings and material before further use. Using low magnification, an imperfection in the AR coating of sample 4 was observed. The extent of the damage to the coating properties could be significant.

The integrating sphere was used extensively for these experiments. Future users may consider obtaining a better mount for the InGaAs detector. While a ring-clamp secured the detector during these experiments, the detector was at risk of becoming detached and falling. Also, the clamp may not have secured the detector in the same manner throughout data collecting allowing for additional background energy to enter the sphere. The use of the lock-in amplifier aided in reducing background noise, so this future design feature is probably needed if the lock-in amplifier is not being used.

The optical quality of OPGaAs must continue to improve. While the thickness of the crystals continue to grow providing a larger usable aperture, the losses due to scattering and absorption are difficult to overcome. Quality of samples and thickness has room for improvement.

Samples 5 and 6 most likely exhibit the same damage threshold since they original from the same vendor. Raising the damage threshold requirement of coatings on future samples is highly recommended.

Better OPO alignment techniques should be investigated with focus on alignment in absence of visual cues. Possible techniques involving an automated feedback mechanism that might aid alignment. Using a small pump laser increases the difficulty of alignment, yet until OPGaAs samples increase in thickness, the pump beam will need to remain small.

The comparisons of multiple OPGaAs samples originating from different manufactures constitute the major findings of this work. Difficulty in manufacturing high quality, thick crystals in numerous quantities is holding back the promise of

OPGaAs. Yet, there remains much potential for OPGaAs and its viability as useful material in future military applications.

Appendix

Figures 25 and 26 each show a set of nine pictures of the beam intensity after propagating through the samples. The camera was not moved during the recording of each set of pictures so any displacement of the beam from center or distortion from nearly circular is due to propagation through the sample. See Figure 11 on page 24 for the image of the beam prior to passing through a sample. The power of the beam was attenuated prior to recording each picture to maximize color contrast of the intensity pattern.

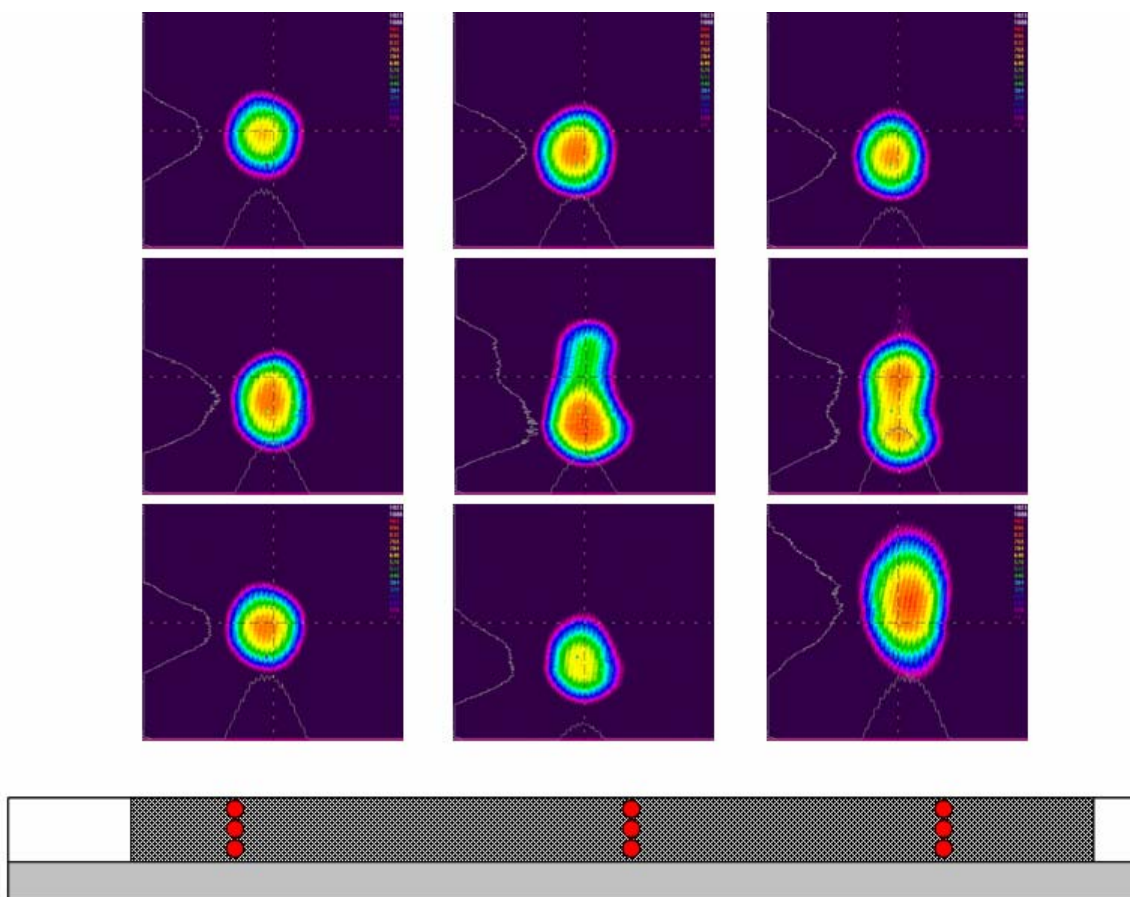


Figure 25: Beam propagation through sample 2.

The nine images of the beam correspond to the nine red circles imposed on the scaled drawing. The placement of the circles shows the approximate location of the beam propagation with respect to the input face of the crystal.

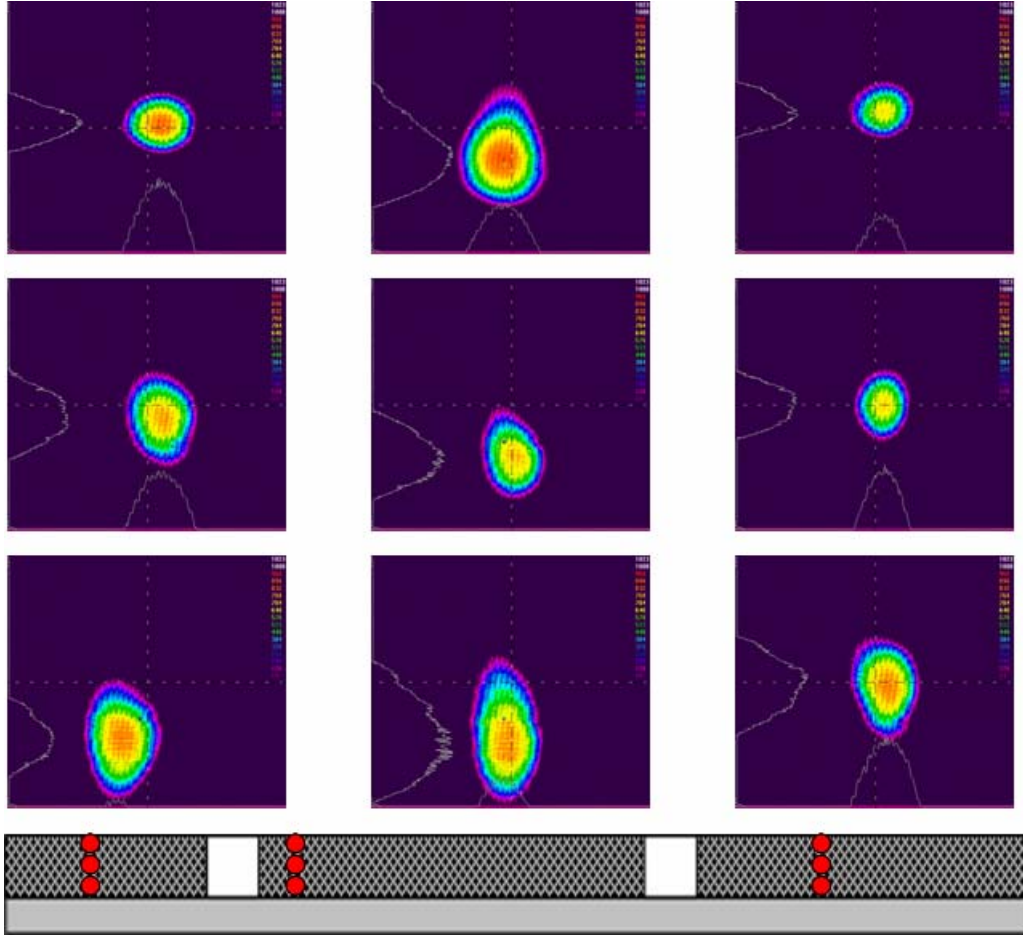


Figure 26: Beam propagation through sample 5.

The nine images of the beam correspond to the nine red circles imposed on the scaled drawing. The placement of the circles shows the approximate location of the beam propagation with respect to the input face of the crystal.

Bibliography

- Armstrong, J., N. Bloembergen, J. Ducuing, and P. S. Pershan. "Interactions between Light Waves in a Nonlinear Dielectric," *Physical Review*. 127, 1918–1939 (1962).
- Bastin, J.A. E.W.J. Mitchell, and J Whitehouse. "Use of an Integrating Sphere to Distinguish Between Absorption and Scattering in Solids," *British Journal of Applied Physics*, Vol. 10, 412-414 (September 1959).
- Boyd, Robert W. *Nonlinear Optics*. New York: Academic Press, 1992.
- Budni, P.A., L.A. Pomeranz, M.L. Lemons, C.A. Miller, J.R. Mosto, and E.P. Chiklis. "Efficient Mid-Infrared Laser Using 1.9- μm -Pumped Ho:YAG and ZnGeP₂ Optical Parametric Oscillators," *Journal of the Optical Society of America - B*, Vol. 17, 723-728 (May 2000).
- Ebert, Christopher. B., Loren A. Eyres, Martin M. Fejer, and James S. Harris, Jr. "MBE Growth of Antiphase GaAs Films Using GaAs/Ge/GaAs Heteroepitaxy," *Journal of Crystal Growth*, 201-202, 187-193 (May 1999).
- Eyres, Loren A., Christopher B. Ebert, Martin M. Fejer, James S. Harris, Jr. "MBE Growth of Laterally Antiphase-Patterned GaAs Films Using Thin Ge Layers for Waveguide Mixing," *Conference on Lasers and Electro-Optics (CLEO 1998)*, 276 (6 May 1998).
- Fejer, Martin .M., "Orientation Patterned Semiconductors: Growth and Applications," Unpublished Briefing, Stanford University, 21 January 2004.
- Franken, P.A., A. E. Hill, C. W. Peters, and G. Weinreich. "Generation of Optical Harmonics," *Physical Review Letters*: 973-976 (1961).
- Giordmaine, J.A. and R.C. Miller, "Tunable Coherent Parametric Oscillation in LiNbO₃ at Optical Frequencies," *Physical Review Letters*: 118-119 (1961).
- Gordon, L., G.L. Woods, R.C. Eckardt, R.R. Route, R.S. Feigelson, M.M Fejer, and R.L. Byer. "Diffusion-bonded stacked GaAs for Quasi-phase matched Second-Harmonic Generation of a Carbon Dioxide laser," *Electronics Letters*, 29, 1942-1944 (28 October 1993).
- Harm, Michael D. *Development of a Tm;Ho:TLF-Laser-Pumped Orientation-Patterned Gallium Arsenide Optical Parametric Oscillator*. Air Force Institute of Technology (AU), Wright Patterson Air Force Base, OH March 2002.

- Harris, Stephen E. "Tunable Optical Parametric Oscillators," *Proceedings of the IEEE*, 57, 2096-2113, (December 1969) in *Selected Papers on Optical Parametric Oscillators and Amplifiers and Their applications*, Vol. MS 140, Jeffery H. Hunt, editor. Bellingham, WA: SPIE Optical Engineering Press, 1997.
- Koh, Shinji, Takashi Knodo, Yasuhiro Shiraki, and Ryoichi Ito. "GaAs/Ge/GaAs Sublattice Reversal Epitaxy and Its Application to Nonlinear Optical Devices," *Journal of Crystal Growth*. 227-228: 183-190 (July 2001).
- Maiman, Theodore H. "Stimulated Optical Radiation in Ruby," *Nature*: 493-494 (1960).
- McMullen, J.D., "Optical Parametric Interactions In Isotropic Materials Using A Phase-Corrected Stack Of Nonlinear Dielectric Plates," *Journal of Applied Physics*: 3076-3081 (1975).
- Myers, L.E., R.C. Eckardt, M.M. Fejer, R.L. Byer, W.R. Bosenberg, J.W. Pierce. "Quasi-Phase-Matched Optical Parametric Oscillators in Bulk Periodically Poled LiNbO₃," *Journal of the Optical Society of America-B*, 12, 2102-2116 (November 1995).
- Peterson, R.D., K.L. Schepler, J.L. Brown, and P.G. Schunemann. "Damage Properties of ZnGeP₂ at 2- μ m," *Journal of the Optical Society of America-B*. 2142-2146 (November, 1995).
- Pinguet, T.J., O. Levi, T. Skauli, L. Eyres, L. Scaccabarozzi, M.M. Fejer, J.S. Harris, T.J. Kulp, S. Bisson, B. Gerard, L. Becouarn, E. Lallier. "Characterization of .5 mm Thick Films of Orientation-Patterned GaAs for Nonlinear Optical Applications," in *OSA Trends in Optics and Photonics Vol. 56., Conference on Lasers and Electro-Optics (CLEO 2001)*, Technical Digest, Postconference Edition. Optical Society of America, Washington, D.C., 138 (2001).
- "Principles of Nonlinear Optical Crystals - Conversion Efficiency," Excerpt from unpublished article. n. pag. <http://www.redoptronics.com/nonlinear-crystal-principal.html>. 13 December 2005.
- Setzler, S.D., G.A. Rines, P.A. Budni, and D.M. Rines. "Efficient ZnGeP₂ Optical Parametric Oscillator in a Doubly Resonant Ring Configuration," *OSA Trends in Optics and Photonics Vol. 68, Advanced Solid-State Lasers*, Martin E. Fermann and Larry R. Marshall eds. Optical Society of America, Washington D.C., 85 (2002).

- Schunemann, P.G., Setzler, S.D. L Mohnkern, T.M. Pollak, D.F. Bliss, D. Weyburne, and K. O'Hearn. "2.05- μm -laser-pumped Orientation-patterned Gallium Arsenide (OPGaAs) OPO," *Optical Society of America* (2005).
- Thompson, D.E., J.D. McMullen, and D.B. Anderson. "Second-Harmonic Generation In GaAs 'Stack Of Plates' Using High-Power CO₂ Laser Radiation," *Applied Physics Letters*: 113-115 (1976).
- Vodopyanov, K.L., F. Ganikhanov, J. P. Fetone, I. Zwieback, and W. Ruderman. "ZnGeP₂ Optical Parametric Oscillator with 3.8 12.4- μm Tunability," *Optics Letters*, 25, 841-843 (2000).
- Vodopyanov K.L., O. Levi, P.S. Kuo, T.J. Pinguet, J.S. Harris, and M.M. Fejer. "Optical Parametric Oscillation in Quasi-phase-matched GaAs," *Optics Letters*. Vol. 29, No. 16, 1912-1914 (August 2004).
- Wolfe, William L. and George J. Zissis. *The Infrared Handbook-Revised Edition*. Washington D.C. Office of Naval Research, Department of the Navy, 1993.
- Yariv, Ammon, Pochi Yeh. *Optical Waves in Crystals-Propagation and Control of Laser Radiation*, New York: Wiley Interscience, 1984.
- Zeigler, B.C. and K.L. Schepler. "Transmission and Damage-Threshold Measurements in AgGaSe₂ at 2.1- μm ," *Applied Optics*, 5077-5080 (December, 1991).

Vita

Captain Joshua W. Meyer graduated from New London-Spicer High School in New London, Minnesota. He received his Bachelor of Arts degree in Physics in May 1996 from the University of Minnesota, Duluth campus. He was commissioned through the Detachment 420 AFROTC at the University of Minnesota, Duluth.

His first assignment was to Shaw AFB, South Carolina as an aircraft maintenance officer in May 1996. His time was not entirely spent in South Carolina as he deployed for 90 days to Incirlik Air Base, Turkey as a sortie generation officer of 12 F-16 aircraft. In January, 1999 he was assigned to Fairchild AFB, Washington in the 92nd Aircraft Generation Squadron as a sortie generation flight commander. While stationed at Fairchild AFB, he deployed to Prince Sultan Air Base, Saudi Arabia for 90 days as the senior maintenance officer for eight KC-135 aircraft. In June, 2001 he was assigned to the Logistics Directorate, Headquarters Air Mobility Command, Scott AFB, Illinois. He served as a staff officer in the Logistics Integration Division and the Aircraft Maintenance Division. In May, 2004 he entered the Graduate School of Engineering and Management, Air Force Institute of Technology. Upon graduation, he will be assigned to the Air Force Office of Scientific Research.

REPORT DOCUMENTATION PAGE				Form Approved OMB No. 074-0188	
<p>The public reporting burden for this collection of information is estimated to average 1 hour per response, including the time for reviewing instructions, searching existing data sources, gathering and maintaining the data needed, and completing and reviewing the collection of information. Send comments regarding this burden estimate or any other aspect of the collection of information, including suggestions for reducing this burden to Department of Defense, Washington Headquarters Services, Directorate for Information Operations and Reports (0704-0188), 1215 Jefferson Davis Highway, Suite 1204, Arlington, VA 22202-4302. Respondents should be aware that notwithstanding any other provision of law, no person shall be subject to a penalty for failing to comply with a collection of information if it does not display a currently valid OMB control number.</p> <p>PLEASE DO NOT RETURN YOUR FORM TO THE ABOVE ADDRESS.</p>					
1. REPORT DATE (DD-MM-YYYY) 15-03-2006		2. REPORT TYPE Thesis		3. DATES COVERED (From – To) May 2004– Mar 2006	
4. TITLE AND SUBTITLE OPTICAL PARAMETRICAL OSCILLATOR DESIGN USING THICK GROWTH ORIENTATION-PATTERNED GALLIUM ARSENIDE				5a. CONTRACT NUMBER	
				5b. GRANT NUMBER	
				5c. PROGRAM ELEMENT NUMBER	
6. AUTHOR(S) Meyer, Joshua W., Captain, USAF				5d. PROJECT NUMBER	
				5e. TASK NUMBER	
				5f. WORK UNIT NUMBER	
7. PERFORMING ORGANIZATION NAMES(S) AND ADDRESS(S) Air Force Institute of Technology Graduate School of Engineering and Management (AFIT/EN) 2950 Hobson Way, Building 640 WPAFB OH 45433-7765				8. PERFORMING ORGANIZATION REPORT NUMBER AFIT/GAP/ENP/06-10	
9. SPONSORING/MONITORING AGENCY NAME(S) AND ADDRESS(ES) AFRL/SNJW Attn: Dr. Rita D. Peterson 2241 Avionics Circle, Building 620 WPAFB OH 45433 DSN: 785-9657 e-mail: Rita.Peterson@wpafb.af.mil				10. SPONSOR/MONITOR'S ACRONYM(S)	
				11. SPONSOR/MONITOR'S REPORT NUMBER(S)	
12. DISTRIBUTION/AVAILABILITY STATEMENT APPROVED FOR PUBLIC RELEASE; DISTRIBUTION UNLIMITED					
13. SUPPLEMENTARY NOTES					
14. ABSTRACT Tunable laser sources in the mid-infrared (MIR) spectral range are required for several Air Force applications. Orientation patterned gallium arsenide (OPGaAs) is a promising nonlinear conversion material because it has broad transparency and can be engineered for specific pump laser and output wavelengths using quasi-phase matching techniques. This research examines the optical quality of seven OPGaAs crystal samples and explores the design of an optical parametric oscillator (OPO) device. Direct transmission and scattering measurements at 2.05-μm were taken as a function of position across the incident face of each sample. Scattering, absorption, and reflection coefficients for each sample were quantified. Nonlinear output from the OPO was not achieved before the optical coating failed. A direct comparison of OPGaAs crystal performance based on source of manufacturing is reported. OPO design parameters are summarized with recommendations for future efforts					
15. SUBJECT TERMS Lasers, Laser Applications, OPGaAs, Orientation Patterned Gallium Arsenide					
16. SECURITY CLASSIFICATION OF:			17. LIMITATION OF ABSTRACT UU	18. NUMBER OF PAGES 69	19a. NAME OF RESPONSIBLE PERSON Lt Col Matthew J. Bohn, (ENP)
a. REPORT U	b. ABSTRACT U	c. THIS PAGE U			19b. TELEPHONE NUMBER (Include area code) (937) 255-3636, ext 4573; e-mail: Matthew.Bohn@afit.edu